Mon. Not. R. Astron. Soc. **000**, 000–000 (0000) Printed 3 September 2009 (MN LATEX style file v2.2)

Simulating the effect of AGN feedback on the metal enrichment of galaxy clusters

D. Fabjan[1,2,3], S. Borgani[1,2,3], L. Tornatore[1,2,3], A. Saro[1,2,3], G. Murante[4] & K. Dolag[5]

[1] *Dipartimento di Astronomia dell'Università di Trieste, via Tiepolo 11, I-34131 Trieste, Italy (fabjan,borgani,tornatore,saro@oats.inaf.it)*
[2] *INAF – Istituto Nazionale di Astrofisica, via Tiepolo 11, I-34131 Trieste, Italy*
[3] *INFN – Istituto Nazionale di Fisica Nucleare, Trieste, Italy*
[4] *INAF – Istituto Nazionale di Astrofisica – Osservatorio Astronomico di Torino, Str. Osservatorio 25, I-10025, Pino Torinese, Torino, Italy (murante@oato.inaf.it)*
[5] *Max-Planck-Institut für Astrophysik, Karl-Schwarzschild Strasse 1, Garching bei München, Germany (kdolag@mpa-garching.mpg.de)*

3 September 2009

ABSTRACT

We present a study of the effect of AGN feedback on metal enrichment and thermal properties of the intracluster medium (ICM) in hydrodynamical simulations of galaxy clusters. The simulations are performed using a version of the TreePM-SPH GADGET-2 code, which also follows chemo-dynamical evolution by accounting for metal enrichment contributed by different stellar populations. We carry out cosmological simulations for a set of galaxy clusters, covering the mass range $M_{200} \simeq (0.1 - 2.2) \times 10^{15}\, h^{-1} M_{\odot}$. Besides runs not including any efficient form of energy feedback, we carry out simulations including three different feedback schemes: *(i)* kinetic feedback in the form of galactic winds triggered by supernova explosions; *(ii)* AGN feedback from gas accretion onto super-massive black holes (BHs); *(iii)* AGN feedback in which a 'radio mode' is included with an efficient thermal coupling of the extracted energy, whenever BHs enter in a quiescent accretion phase. Besides investigating the resulting thermal properties of the ICM, we analyse in detail the effect that these feedback models have on the ICM metal-enrichment. We find that AGN feedback has the desired effect of quenching star formation in the brightest cluster galaxies at $z < 4$ and provides correct temperature profiles in the central regions of galaxy groups. However, its effect is not yet sufficient to create "cool cores" in massive clusters, while generating an excess of entropy in central regions of galaxy groups. As for the pattern of metal distribution, AGN feedback creates a widespread enrichment in the outskirts of clusters, thanks to its efficiency in displacing enriched gas from galactic halos to the inter-galactic medium. This turns into profiles of Iron abundance, $Z_{\rm Fe}$, which are in better agreement with observational results, and into a more pristine enrichment of the ICM around and beyond the cluster virial regions. Following the pattern of the relative abundances of Silicon and Iron, we conclude that a significant fraction of the ICM enrichment is contributed in simulations by a diffuse population of intra-cluster stars. Our simulations also predict that profiles of the $Z_{\rm Si}/Z_{\rm Fe}$ abundance ratio do not increase at increasing radii, at least out to $0.5R_{vir}$. Our results clearly show that different sources of energy feedback leave distinct imprints in the enrichment pattern of the ICM. They further demonstrate that such imprints are more evident when looking at external regions, approaching the cluster virial boundaries.

Key words: Cosmology: Theory – Methods: Numerical – X–Rays: Galaxies: Clusters – Galaxies: Abundances – Galaxies: Intergalactic Medium

1 INTRODUCTION

High quality data from the current generation of X–ray satellites (XMM-Newton, Chandra and Suzaku) have now established a number of observational facts concerning the thermo-dynamical and chemo-dynamical properties of the intra-cluster medium (ICM) for statistically representative sets of galaxy clusters: core regions of relaxed clusters show little evidence of gas cooler than about a third of the virial temperature (e.g., Peterson et al. 2001; Böhringer et al. 2002; Sanderson et al. 2006); temperature profiles have negative gradients outside core regions, a trend that extends out to the largest radii covered so far by observations (e.g., De Grandi & Molendi 2002; Vikhlinin et al. 2005; Zhang et al. 2006; Baldi et al. 2007; Pratt et al. 2007; Leccardi & Molendi

2008b); gas entropy is higher than expected from simple self-similar scaling properties of the ICM, not only in core regions, but also out to R_{500}[1] (e.g., Sun et al. 2009, and references therein); radial profiles of the Iron abundance show negative gradients, more pronounced for relaxed "cool core" clusters, with central values of $Z_{\rm Fe}$ approaching solar abundance and with a global enrichment at a level of about 1/3–1/2 $Z_{Fe,\odot}$ (e.g.,De Grandi et al. 2004; Vikhlinin et al. 2005; de Plaa et al. 2006; Snowden et al. 2008; Leccardi & Molendi 2008a; see Mushotzky 2004; Werner et al. 2008 for recent reviews).

Galaxy clusters arise from the collapse of density perturbations over a scale of $\sim 10\,h^{-1}$ comoving Mpc. As such, the above observational properties of the ICM come from a non-trivial interplay between the underlying cosmological scenario, which shapes the large-scale structure of the Universe, and a number of astrophysical processes (e.g., star formation, energy and chemical feedback from supernovae and AGN) taking place on much smaller scales. Cosmological hydrodynamical simulations represent the modern instrument with which such complexities can be described as the result of hierarchical assembly of cosmic structures (e.g., Borgani & Kravtsov 2009, for a recent review). Indeed, simulations of galaxy clusters reach nowadays a high enough resolution, while including a realistic description of the above mentioned astrophysical processes, for them to provide a coherent interpretative framework for X-ray observations. Quite remarkably, simulation predictions for the thermodynamical properties of the ICM are in good agreement with observations, at least outside the core regions: simulated profiles of gas density and temperature match the observed ones at cluster-centric distances $\gtrsim 0.1R_{500}$ (e.g., Loken et al. 2002; Borgani et al. 2004; Kay et al. 2004; Roncarelli et al. 2006; Pratt et al. 2007; Nagai et al. 2007; Croston et al. 2008); the observed entropy level at R_{500} is well reproduced by simulations including radiative cooling and star formation (e.g., Nagai et al. 2007; Borgani & Viel 2009). The situation is quite different within cluster cores, where simulations including only stellar feedback generally fail at producing realistic cool cores. The two clearest manifestations of this failure are represented by the behaviour of temperature and entropy profiles at small radii, $\lesssim 0.1R_{500}$. Observations of cool core clusters show that temperature profiles smoothly decline toward the centre, reaching temperatures of about 1/3–1/2 of the maximum value, while the entropy level at the smallest sampled scales is generally very low (e.g., Sun et al. 2009; Sanderson et al. 2009a). On the contrary, radiative simulations including a variety of models of stellar feedback predict steep negative temperature gradients down to the innermost resolved radii and central entropy levels much higher than observed (e.g., Valdarnini 2003; Tornatore et al. 2003; Borgani et al. 2004; Nagai et al. 2007; cf. also Kay et al. 2007). This failure of simulations is generally interpreted as due to overcooling, which takes place in simulated clusters even when including an efficient supernova (SN) feedback, and causes an excess of star formation in the simulated brightest cluster galaxies (BCGs; Romeo et al. 2005; Saro et al. 2006).

The generally accepted solution to these shortcomings of simulations is represented by AGN feedback. Indeed, the presence of cavities in the ICM at the cluster centre is considered as the fingerprint of the conversion of mechanical energy associated to AGN jets into thermal energy (and possibly in a non–thermal content of relativistic particles) through shocks (e.g., Mazzotta et al. 2004; Fabian et al. 2005; McNamara et al. 2006; Sanders & Fabian 2007; see McNamara & Nulsen 2007 for a review). Although analytical arguments convincingly show that the energy radiated from gas accretion onto a central super-massive black hole (BH) is enough to suppress gas cooling, it is all but clear how this energy is thermalised and distributed in the surrounding medium. A likely scenario is that bubbles of high entropy gas are created at the termination of jets. Buoyancy of these bubbles in the ICM then distributes thermal energy over larger scales (e.g., Dalla Vecchia et al. 2004; Cattaneo et al. 2007). Crucial in this process is the stability of the bubbles against gas dynamical instabilities which would tend to destroy them quite rapidly. Indeed, detailed numerical simulations have demonstrated that gas circulation associated to jets (e.g., Omma et al. 2004; Brighenti & Mathews 2006; Heinz et al. 2006), gas viscosity, magnetic fields (e.g., Ruszkowski et al. 2007) and injection of cosmic rays (e.g., Ruszkowski et al. 2008) are all expected to cooperate in determining the evolution of buoyant bubbles. Although highly instructive, all these simulations have been performed for isolated halos and, as such, they describe neither the cosmological growth and merging of black holes, nor the hierarchical assembly of galaxy clusters.

Springel et al. (2005) and Di Matteo et al. (2005) have presented a model that follows in a cosmological simulation the evolution of the BH population and the effect of energy feedback resulting from gas accretion onto BHs. In this model, BHs are treated as sink particles which accrete from the surrounding gas according to a Bondi accretion rate (e.g., Bondi 1952), with an upper limit provided by the Eddington rate (see also Booth & Schaye 2009). This model was used by Bhattacharya et al. (2008), who run cosmological simulations to study the effect of AGN feedback on galaxy groups. They found that this feedback is effective in reducing star formation in central regions and to displace gas towards outer regions. However, the resulting entropy level within cluster cores is higher than observed. In its original version, the energy extracted from BH accretion is locally distributed to the gas around the BHs according to a SPH-kernel weighting scheme. This model has been modified by Sijacki & Springel (2006) who included the possibility to inflate high-entropy bubbles in the ICM whenever accretion onto the central BH enters in a quiescent "radio mode". The underlying idea of injecting bubbles with this prescription was to provide a more realistic description of the effect of jet termination on the ICM, although the effect of the jet itself was not included. Puchwein et al. (2008) simulated a set of clusters and groups to show that this feedback scheme is able to reproduce the observed slope of the relation between X–ray luminosity and temperature. Sijacki et al. (2007) showed in a simulation of a single poor galaxy cluster that the injection of bubbles is quite effective in suppressing star formation in central regions. However, also in this case the temperature profile in the core regions does not match the observed slope, while more realistic temperature profiles can be produced if bubble injection is associated to the injection of a non–thermal population of relativistic particles (Pfrommer et al. 2007; Sijacki et al. 2008). Although these authors presented results concerning the effect of AGN on the ICM thermodynamics, no detailed analysis has been so far carried out to study the interplay between AGN and chemical enrichment, by including a detailed chemo-dynamical description of the ICM.

Indeed, the amount and distribution of metals in the ICM provide an important diagnostic to reconstruct the past history of star

[1] Here and in the following we will indicate with R_Δ the radius encompassing a mean density equal to $\Delta\rho_{cr}$, being $\rho_{cr} = 3H^2/8\pi G$ the critical cosmic density. In a similar way, we will indicate with M_Δ the mass contained within R_Δ.

formation and the role of gas-dynamical and feedback processes in displacing metals from star forming regions (e.g., Mushotzky 2004; Borgani et al. 2008; Schindler & Diaferio 2008, for reviews). Cosmological chemo-dynamical simulations of galaxy clusters generally show that the predicted profiles of Iron abundance are steeper than observed (e.g., Valdarnini 2003; Tornatore et al. 2004; Romeo et al. 2005; Tornatore et al. 2007; Davé et al. 2008), with an excess of enrichment in the core regions. This is generally interpreted as due to the same excess of recent star formation in simulated BCGs. However, Fabjan et al. (2008) showed that an excess of recent star formation has also the effect of efficiently locking recently-produced metals into stars, thereby preventing a too fast increase of the metallicity of the hot diffuse medium.

All the above analyses are based on different implementations of SN energy feedback, while only much less detailed analyses of ICM metal enrichment have been so far presented by also including AGN feedback in cosmological simulations (e.g., Sijacki et al. 2007; Moll et al. 2007). For instance, Roediger et al. (2007) showed from simulations of isolated halos that buoyancy of bubbles can actually displace a large amount of the central highly enriched ICM, thus leading to a radical change of the metallicity profiles, or even to a disruption of the metallicity gradients.

The aim of this paper is to present a detailed analysis of cosmological hydrodynamical simulations of galaxy clusters, which have been carried out with the GADGET-2 code (Springel 2005), by combining the AGN feedback model described by Springel et al. (2005) with the SPH implementation of chemo-dynamics presented by Tornatore et al. (2007). Besides showing results on the effect of combining metallicity–dependent cooling and AGN feedback on the ICM thermodynamics, we will focus our discussion on the different effects that SNe and AGN feedback have on the chemical enrichment of the ICM. Although we will shortly discuss the effect of different feedback sources on the pattern of star formation in the BCG, the results presented in this paper will mainly concern the enrichment of the hot diffuse intra-cluster gas. We defer to a forthcoming paper a detailed analysis of the effect of AGN feedback on the population of cluster galaxies. The scheme of the paper is as follows. We present in Section 2 the simulated clusters, and briefly describe the implementation of the chemical evolution model in the GADGET-2 code along with the SN and AGN feedback models. In Section 3 we show our results on the thermal properties of the ICM and their comparison with observational results. Section 4 is devoted to the presentation of the results on the ICM chemical enrichment from our simulations and their comparison with the most recent observations. We discuss our results and draw our main conclusions in Section 5.

2 THE SIMULATIONS

2.1 The set of simulated clusters

Our set of simulated clusters is obtained from nine Lagrangian regions extracted from a simulation containing only dark matter (DM) with a box size of 479 h^{-1} Mpc (Yoshida et al. 2001), performed for a flat Λ cold dark matter (CDM) cosmological model with relevant parameters $\Omega_m = 0.3$, $\mathrm{h}_{100} = 0.7$, $\sigma_8 = 0.9$. This set of simulated clusters is described in detail by Dolag et al. (2008). The regions are centred on nine galaxy clusters: five of them have masses $M_{200} \simeq 1.0 \times 10^{14}\, h^{-1} M_\odot$, while the remaining four have $M_{200} \simeq (1.0 - 2.2) \times 10^{15}\, h^{-1} M_\odot$. The regions of three largest objects also contain other clusters, so that we have in total 18 clusters with $M_{200} \gtrsim 5 \times 10^{13}\, h^{-1} M_\odot$, whose basic characteristics are reported in Table 1.

Table 1. Characteristics of the simulated clusters. Column 1: cluster name. Column 2: mass contained within R_{200} (units of $10^{14}\, h^{-1} M_\odot$). Column 3: value of R_{200} (units of $h^{-1}\mathrm{Mpc}$). Column 4: value of the spectroscopic-like temperature within R_{500}, T_{500}. Columns 5 and 6: mass of the central BH hosted in the BCG for the AGN1 and AGN2 runs (units of $10^{10}\, h^{-1} M_\odot$), respectively. For the g51 cluster, the two additional values reported for the mass of the central BH refer to the AGN2(0.8) and AGN2W runs (see text) and are indicated with the † and ‡ symbol, respectively.

Cluster	M_{200}	R_{200}	T_{500}	M_{BH}	
				AGN1	AGN2
g1.a	12.69	1.76	9.71	56.22	15.74
g1.b	3.64	1.16	3.39	7.96	2.52
g1.c	1.36	0.84	2.03	4.63	1.32
g1.d	1.04	0.76	1.82	1.59	0.46
g1.e	0.62	0.64	1.44	0.84	0.30
g8.a	18.51	2.00	12.82	113.50	27.73
g8.b	0.65	0.65	1.41	2.58	0.88
g8.c	0.52	0.61	1.42	1.74	0.63
g51	10.95	1.68	7.55	43.38	16.50 6.18† 15.02‡
g72.a	10.57	1.66	8.67	48.74	13.87
g72.b	1.48	0.86	2.18	3.79	1.34
g676	0.87	0.72	1.91	3.03	0.95
g914	0.88	0.72	2.03	2.89	1.13
g1542	0.83	0.71	1.79	2.54	0.79
g3344	0.92	0.74	2.03	3.15	1.29
g6212	0.89	0.73	2.02	2.57	0.99

Table 2. Resolution of the different runs. Column 2-3: mass of the DM particles and initial mass of the gas particles (units of $10^8\, h^{-1} M_\odot$). Column 4: value of the Plummer-equivalent gravitational force softening at $z = 0$ (units of $h^{-1}\mathrm{kpc}$). Column 5: clusters simulated at each resolution.

	M_{DM}	m_{gas}	ε	Clusters
Low res.	11.0	2.03	5.00	g1, g8, g51, g72, g676
High res.	1.69	0.31	2.75	g676, g914, g1542, g3344, g6212

Each region was re-simulated using the zoomed initial condition (ZIC) technique by Tormen et al. (1997). The relative mass of the gas and dark matter (DM) particles within the high–resolution region of each simulation is set so that $\Omega_{bar} = 0.045$ for the density parameter contributed by baryons. For each Lagrangian region, initial conditions have been generated at a basic resolution and at 6.5 times higher mass resolution. At this higher resolution, the mass of the DM and gas particles are $m_{DM} \simeq 1.9 \times 10^8\, h^{-1} M_\odot$ and $m_{gas} = 2.8 \times 10^7\, h^{-1} M_\odot$ respectively, with Plummer equivalent softening length for the computation of the gravitational force set to $\varepsilon = 2.75\, h^{-1}\mathrm{kpc}$ in physical units below $z = 2$ and to $\varepsilon = 8.25\, h^{-1}\mathrm{kpc}$ in comoving units at higher redshifts. In the lower resolution runs, these values are rescaled according to $m_{DM}^{-1/3}$. We decided to simulate the nine Lagrangian regions with massive clusters at the lower resolution, while we used the higher resolution for the five low-mass clusters. Only the low-mass g676 cluster was simulated at both resolutions. We provide in Table 2 a description of the parameters for the two different resolutions, also listing the clusters simulated at each resolution.

2.2 The simulation code

Our simulations were performed using the TreePM-SPH GADGET-2 code (Springel 2005). All simulations include a metallicity-dependent radiative cooling (Sutherland & Dopita 1993), heating from a uniform time-dependent ultraviolet background (Haardt & Madau 1996) and the effective model by Springel & Hernquist (2003) for the description of star formation. In this model, gas particles above a given density are treated as multiphase, so as to provide a sub–resolution description of the inter-stellar medium. In the following, we assume the density threshold for the onset of star formation in multiphase gas particles to be $n_H = 0.1cm^{-3}$ in terms of number density of hydrogen atoms. Our simulations also include a detailed model of chemical evolution by Tornatore et al. (2007, T07 hereafter). We address the reader to T07 for a more detailed description of this model. Metals are produced by SNe-II, SNe-Ia and intermediate and low-mass stars in the asymptotic giant branch (AGB hereafter). We assume SNe-II to arise from stars having mass above $8M_{\odot}$. As for the SNe-Ia, we assume their progenitors to be binary systems, whose total mass lies in the range (3–16)$M_{\odot}$. Metals and energy are released by stars of different mass by properly accounting for mass–dependent lifetimes. In this work we assume the lifetime function proposed by Padovani & Matteucci (1993), while we assume the standard stellar initial mass function (IMF) by Salpeter (1955). We adopt the metallicity–dependent stellar yields by Woosley & Weaver (1995) for SNe-II, the yields by van den Hoek & Groenewegen (1997) for the AGB and by Thielemann et al. (2003) for SNe-Ia. The version of the code used for the simulations presented here allowed us to follow H, He, C, O, Mg, S, Si and Fe. Once produced by a star particle, metals are then spread to the surrounding gas particles by using the B-spline kernel with weights computed over 64 neighbours and taken to be proportional to the volume of each particle (see T07 for detailed tests on the effect of choosing different weighting schemes to spread metals).

2.3 Feedback models

In the simulations presented in this paper we model two different sources of energy feedback. The first one is the kinetic feedback model implemented by Springel & Hernquist (2003), in which energy released by SN-II triggers galactic winds, with mass upload rate assumed to be proportional to the star formation rate, $\dot{M}_W = \eta \dot{M}_{\star}$. Therefore, fixing the parameter η and the wind velocity v_W amounts to fix the total energy carried by the winds. In the following, we assume $\eta = 2$ for the mass-upload parameter and $v_W = 500\,\mathrm{km\,s^{-1}}$ for the wind velocity. If each SN-II releases 10^{51} ergs, the above choice of parameters corresponds to assuming that SNe-II power galactic outflows with nearly unity efficiency for a Salpeter IMF (see Springel & Hernquist 2003).

Furthermore, we include in our simulations the effect of feedback energy released by gas accretion onto super-massive black holes (BHs), following the scheme originally introduced by Springel et al. (2005, SDH05 hereafter; see also Di Matteo et al. 2005, 2008; Booth & Schaye 2009). We refer to SDH05 for a more detailed description. In this model, BHs are represented by collisionless sink particles of initially very small mass, that are allowed to subsequently grow via gas accretion and through mergers with other BHs during close encounters. During the growth of structures, we seed every new dark matter halo above a certain mass threshold M_{th}, identified by a run-time friends-of-friends algorithm, with a central BH of mass $10^5\,h^{-1}M_{\odot}$, provided the halo does not contain any BH yet. For the runs at the lower resolution the value of the halo mass assumed to seed BHs is $M_{th} = 5 \times 10^{10}\,h^{-1}M_{\odot}$, so that it is resolved with about 40 DM particles. At the higher resolution the halo mass threshold for BH seeding decreases to $M_{th} = 10^{10}\,h^{-1}M_{\odot}$, so as to resolve it with approximately the same number of particles. We verified that using in the higher-resolution runs the same value of M_{th} as in the low-resolution runs causes the effect of BH accretion to be shifted toward lower redshift, since its onset has to await the formation of more massive halos, while leaving the final properties of galaxy clusters almost unaffected.

Once seeded, each BH can then grow by local gas accretion, with a rate given by

$$\dot{M}_{BH} = \min\left(\dot{M}_B, \dot{M}_{Edd}\right) \tag{1}$$

or by merging with other BHs. Here $\dot{M}_B$ is the accretion rate estimated with the Bondi-Hoyle-Lyttleton formula (Hoyle & Lyttleton 1939; Bondi & Hoyle 1944; Bondi 1952), while $\dot{M}_{Edd}$ is the Eddington rate. The latter is inversely proportional to the radiative efficiency ϵ_r, which gives the radiated energy in units of the energy associated to the accreted mass:

$$\epsilon_r = \frac{L_r}{\dot{M}_{BH}c^2}\,. \tag{2}$$

Following Springel et al. (2005), we use $\epsilon_r = 0.1$ as a reference value, which is typical for a radiatively efficient accretion onto a Schwartzschild BH (Shakura & Syunyaev 1973). The model then assumes that a fraction ϵ_f of the radiated energy is thermally coupled to the surrounding gas, so that $\dot{E}_{\rm feed} = \epsilon_r\epsilon_f\dot{M}_{BH}c^2$ is the rate of provided energy feedback. In standard AGN feedback implementation we use $\epsilon_f = 0.05$ following Di Matteo et al. (2005), who were able with this value to reproduce the observed $M_{BH} - \sigma$ relation between bulge velocity dispersion and mass of the hosted BH (e.g., Magorrian et al. 1998). This choice was also found to be consistent with the value required in semi-analytical models to explain the evolution of the number density of quasars (Wyithe & Loeb 2003).

Gas swallowed by the BH is implemented in a stochastic way, by assigning to each neighbour gas particle a probability of contributing to the accretion, which is proportional to the SPH kernel weight computed at the particle position. Differently from SDH05, we assume that each selected gas particle contributes to the accretion with 1/3 of its mass, instead of being completely swallowed. In this way, a larger number of particles contribute to the accretion, which is then followed in a more continuous way. We remind that in the SDH05 scheme, this stochastic accretion is used only to increase the dynamic mass of the BHs, while their mass entering in the computation of the accretion rate is followed in a continuous way, by using the analytic expression for $\dot{M}_{BH}$. Once the amount of energy to be thermalised is computed for each BH at a given time-step, one has to distribute this energy to the surrounding gas particles. In their original formulation, SDH05 distributed this energy using the SPH kernel.

Besides following this standard implementation of the AGN feedback, we also follow an alternative prescription, which differ from the original one in two aspects.

Firstly, following Sijacki et al. (2007), we assume that a transition from a "quasar" phase to "radio" mode of the BH feedback takes place whenever the accretion rate falls below a given limit (e.g., Churazov et al. 2005, and references therein), corresponding to $\dot{M}_{BH}/\dot{M}_{Edd} < 10^{-2}$, which implies an increase of the feed-

back efficiency to $\epsilon_f = 0.2$. At high redshift BHs are characterised by high accretion rates and power very luminous quasars, with only a small fraction of the radiated energy being thermally coupled to the surrounding gas. On the other hand, BHs hosted within very massive halos at lower redshift are expected to accrete at a rate well below the Eddington limit, while the energy is mostly released in a kinetic form, eventually thermalised in the surrounding gas through shocks. Secondly, instead of distributing the energy using a SPH kernel, we distribute it using a top-hat kernel, having radius given by the SPH smoothing length. In order to avoid spreading the energy within a too small sphere, we assume a minimum spreading length of $2\,h^{-1}$kpc. The rationale behind the choice of the top-hat kernel is to provide a more uniform distribution of energy, thus mimicking the effect of inflating bubbles in correspondence of the termination of the AGN jets. It is well known that a number of physical processes need to be adequately included for a fully self-consistent description of bubble injection and buoyancy: gas-dynamical effects related to jets, magnetic fields, viscosity, thermal conduction, injection of relativistic particles.

In particular, a number of studies based on simulations of isolated halos (e.g., Omma et al. 2004; Brighenti & Mathews 2006) have pointed out that gas circulation generated by jets provides an important contribution for the stabilization of cooling flows (see also Heinz et al. 2006, for a cosmological simulation of cluster formation including jets). In its current implementation, the model of BH feedback included in our simulations neglects any kinetic feedback associated to jets. Based on an analytical model, Pope (2009) computed the typical scale of transition from kinetic to thermal feedback regime for AGN in elliptical galaxies and clusters. As a result, he found that the effect of momentum carried by jets can be neglected on scales $\gtrsim 20$ kpc, the exact value depending on the local conditions of the gas and on the injection rate of kinetic and thermal energy. In order to compare such a scale to that actually resolved in our simulations, we remind the reader that SPH hydrodynamics is numerically converged on scales about 6 times larger than the Plummer–equivalent softening scale for gravitational force (e.g., Borgani et al. 2002). Owing to the values of the gravitational softening reported in Table 2, the scales resolved in our simulations are not in the regime where kinetic feedback is expected to dominate, thus justifying the adoption of a purely thermal feedback. As a further test, we have computed the radius of the top–hat kernel within which energy is distributed around the central BHs in our simulated clusters. As a few examples, we found at $z = 0$ this radius to be 21 kpc and 23 kpc for the AGN2 runs of the g72 and g676 clusters, respectively. This implies that we are in fact distributing thermal energy over scales where kinetic feedback should not be dominant.

In view of the difficulty of self–consistently including the cooperative effect of all the physical processes we listed above, we prefer here to follow a rather simplified approach and see to what extent [results on] the final results of our simulations are sensitive to variations in the implementation of the BH feedback model.

In summary, we performed four series of runs, corresponding to as many prescription for energy feedback.

(a) No feedback (NF hereafter): neither galactic winds nor AGN feedback is included.

(b) Galactic winds (W hereafter) included by following the model by Springel & Hernquist (2003), with $v_w = 500\,\mathrm{km\,s^{-1}}$ and $\eta = 2$ for the wind mass upload.

(c) Standard implementation of AGN feedback from BH accretion (AGN1 hereafter), using $\epsilon_f = 0.05$ for the feedback efficiency.

(d) Modified version of the AGN feedback (AGN2 hereafter), with feedback efficiency increasing from $\epsilon_f = 0.05$ to $\epsilon_f = 0.2$ when $\dot{M}_{BH}/\dot{M}_{Edd} < 10^{-2}$, and distribution of energy around the BH with a top-hat kernel.

In order to further explore the parameter space of the considered feedback models we also carried out one simulation of the g51 cluster based on the AGN2 scheme, but with the feedback efficiency increased to $\epsilon_f = 0.8$ (AGN2(0.8) hereafter). We also note that our simulations include either winds triggered by SN explosions or AGN feedback. While this choice is done with the purpose of separate the effects of these two feedback sources, we expect in realistic cases that both AGN and SN feedback should cooperate in determining the star formation history of galaxies. In order to verify the effect of combining the two feedback sources, we carried out one simulation of the AGN2 scheme for the g51 cluster, in which also galactic winds with a velocity $v_w = 300\,\mathrm{km\,s^{-1}}$ are included (AGN2W hereafter).

Before starting the presentation of the results on the thermal and enrichment properties of the ICM, we briefly comment on the results concerning the mass of the central black holes in the simulations including AGN feedback, and the star formation rate (SFR) history of the brightest cluster galaxies (BCGs).

Looking at Table 1, we note that our simulations predict rather large masses for the super-massive BHs hosted in the central galaxies. Quite interestingly, the AGN2 runs generally produce BH masses which are smaller, by a factor 3–5, than for the AGN1 runs. This demonstrates that including the more efficient "radio mode" for the feedback and distributing the energy in a more uniform way has a significant effect in regulating gas accretion. Although BCGs are known to host BHs which are more massive than expected for normal early type galaxies of comparable mass (e.g., Lauer et al. 2007), the BH masses from our simulations seem exceedingly large, also for the AGN2 model. For instance, the BH mass hosted by M87, within the relatively poor Virgo cluster, is $m_{BH} \simeq (3-4) \times 10^9 M_\odot$ (e.g., Rafferty et al. 2006). This is about a factor 3–5 smaller than found in our AGN2 runs for clusters of comparable mass, $M_{200} \simeq 2 \times 10^{14}\,h^{-1} M_\odot$. We note that increasing the radio-mode feedback efficiency from $\epsilon_f = 0.2$ to 0.8 (AGN2(0.8) run) reduces the mass of the central black hole in the g51 cluster from $m_{BH} \simeq 16.5 \times 10^9 M_\odot$ to $\simeq 6.2 \times 10^9 M_\odot$ (see Table 1). This suggests that a highly efficient thermalization of the energy extracted from the BH is required to regulate gas accretion to the observed level. Quite interestingly, we also note that adding the effect of galactic winds in the AGN2 scheme (AGN2W run) only provides a marginal reduction of the final mass of the central BH. Therefore, although galactic winds can play a significant role in regulating star formation within relatively small galaxies, they are not efficient in decreasing gas density around the largest BHs, so as to suppress their accretion rate.

As for the comparison with previous analyses, Sijacki et al. (2007) performed a simulation of the same g676 cluster included in our simulation set at the lower resolution, for their feedback scheme based on the injection of AGN driven bubbles. They found that the final mass of the central BH is $m_{BH} \simeq 6 \times 10^9\,h^{-1} M_\odot$. This value is about 30 per cent lower than what we find for the AGN2 runs of g676. In order to compare more closely with the result by Sijacki et al. (2007), we repeated the run of the g676 cluster by switching off the metallicity-dependence of the cooling function. As a result, BH accretion proceeds in a less efficient way, and the resulting central BH mass in this case drops to $\simeq 3.5 \times 10^9\,h^{-1} M_\odot$.

As for the SFR history of the BCG, this is estimated by identifying first all the stars belonging to the BCG at $z = 0$. This has been done by running the SKID group-finding algorithm (Stadel 2001), using the same procedure described by Saro et al. (2006). After tagging all the star particles belonging to the BCG, we reconstruct the SFR history by using the information on the redshift at which each star particle has been spawned by a parent gas particle, according to the stochastic algorithm of star formation implemented in the effective model by Springel & Hernquist (2003). The resulting SFR histories for the BCG of the g51 clusters are shown in the left panel of Figure 1.

As expected, the run with no efficient feedback (NF) produces the highest star formation at all epochs: SFR has a peak at $z \simeq 4$ and then drops as a consequence of the exhaustion of gas with short cooling time. Despite this fast reduction of the SFR, its level at $z = 0$ is still rather large, $\simeq 400\, h^{-1} M_{\odot}$ yr^{-1}. As for the run with winds, it has a reduced SFR since the very beginning, owing to the efficiency of this feedback scheme in suppressing star formation within small galaxies which form already at high redshift. Also in this case, the peak of star formation takes place at $z \sim 4$, but with an amplitude which is about 40 per cent lower than for the NF runs and with a more gentle decline afterwards. As for the runs with AGN feedback, their SFR history is quite similar to that of the W run down to $z \simeq 5$. Star formation is then suddenly quenched at $z \lesssim 4$. We note in general that SFR for the AGN1 model lies slightly below that of the AGN2 model, as a consequence of both the different way of distributing energy and, at low redshift, of the inclusion of the radio mode assumed in the quiescent BH accretion phase. Suppression of the SF at relatively low redshift is exactly the welcome effect of AGN feedback. At $z = 0$, the resulting SFR is of about $70 M_{\odot}$yr^{-1} for both models, a value which is closer to, although still higher than the typical values of SFR observed in the BCGs of clusters of comparable mass. (e.g., Rafferty et al. 2006). Quite interestingly, increasing the feedback efficiency to $\epsilon_f = 0.8$ in the AGN2(0.8) run does not significantly affect the level of low-redshift star formation, while it suppresses star formation by only ~ 10 per cent around the peak of efficiency. Therefore, while a higher efficiency is indeed effective in suppressing gas accretion onto the central BH, a further reduction of star formation associated to the BCG should require a different way of thermalizing the radiated energy. As for the AGN2W run, its SFR at high redshift is lower than for the AGN2 run, due to the effect of winds, while no significant change is observed at $z \lesssim 3$.

In the right panel of Fig.1 we plot the stellar mass found in the BCG at $z = 0$ that is formed before a given redshift. According to this definition, this quantity is the integral of the SFR plotted in the right panel, computed from a given redshift z to infinity. This plot clearly shows the different effect that winds and AGN feedback have in making the BGC stellar population older. In the NF and W runs, the redshift at which 50 per cent of the BCG stellar mass was already in place is $z_{50} \simeq 2$. This indicates that even an efficient SN feedback is not able to make the stellar population of the BCG older. On the contrary, the effect of AGN feedback takes place mostly at relatively low reshift. As a consequence the age of the BGC stellar population increases, with $z_{50} \simeq 3.0 - 3.6$, almost independent of the detail of the AGN feedback scheme.

3 THERMAL PROPERTIES OF THE ICM

Galaxy clusters are identified in each simulation box by running first a friends-of-friends (FOF) algorithm over the high resolution DM particles, using a linking length of 0.15 in terms of the mean inter-particle separation. Within each FOF group, we identify the DM particle having the minimum value of the gravitational potential and take its position to correspond to the centre of the cluster. All profiles are then computed starting from this centre. The smallest radius that we use to compute profiles encompasses a minimum number of 100 SPH particles, a criterion that gives numerically converged results for profiles of gas density and temperature in non–radiative simulations (e.g., Borgani et al. 2002). As we shall see in the following, profiles computed with this criterion will extend to smaller radii for those runs which have a higher gas density at the centre, while stopping at relatively larger radii for the runs including AGN feedback, which are characterised by a lower central gas density.

3.1 The luminosity-temperature relation

The relation between bolometric X–ray luminosity, L_X and ICM temperature, T, provided one of the first evidences that non–gravitational effects determine the thermo-dynamical properties of the ICM (e.g., Voit 2005, for a review). Its slope at the scale of clusters is observed to be $L_X \propto T^{\alpha}$ with $\alpha \simeq 2.5$–3 (e.g., Horner 2001; Pratt et al. 2009), and possibly even steeper or with a larger scatter at the scale of galaxy groups (e.g., Osmond & Ponman 2004). These results are at variance with respect to the prediction, $\alpha = 2$, of self-similar models based only on the effect of gravitational gas accretion (e.g., Kaiser 1986). Attempts to reproduce the observed L_X–T relation with hydrodynamic simulations of clusters have been pursued by several groups (see Borgani et al. 2008, for a recent review). Simulations of galaxy clusters including the effect of star formation and SN feedback in the form of energy–driven galactic winds produce results which are close to observations at the scale of clusters, while generally producing too luminous galaxy groups (e.g., Borgani et al. 2004). Although a closer agreement with observations at the scale of groups can be obtained by using SN–triggered momentum–driven winds (Davé et al. 2008), there is a general consensus that stellar feedback can not reproduce at the same time both the observed L_X–T relation and the low star formation rate observed in central cluster galaxies. Puchwein et al. (2008) presented results on the L_X–T relation for simulations of galaxy clusters which included the bubble–driven AGN feedback scheme introduced by Sijacki et al. (2007). They concluded that, while simulations not including any efficient feedback (in fact, quite similar to our NF runs) produce overluminous objects, their mechanism for AGN feedback is efficient in suppressing the X–ray luminosity of clusters and groups at the observed level.

We present here our results on the L_X–T relation, keeping in mind that our simulations differ from those by Puchwein et al. (2008) both in the details of the implementation of the AGN feedback scheme and in the treatment of the metallicity dependence of the cooling function. In the left panel of Figure 2 we show the results for our runs based on SN galactic winds (W runs) and for the runs not including any efficient feedback (NF runs). Filled symbols refer to the main halo of each simulated Lagrangian region, while open circles are for the "satellites". Although we find several satellites having a temperature comparable to those of the low-mass main halos (see also Table 1), we remind that these satellites are described with a mass resolution six times lower than that of the low-mass main halos. We note that the NF runs provide a L_X–T relation which is not far from the observed one, especially at the scale of groups. The reason for this closer agreement, with respect to the result by Puchwein et al. (2008) lies in the fact that these authors

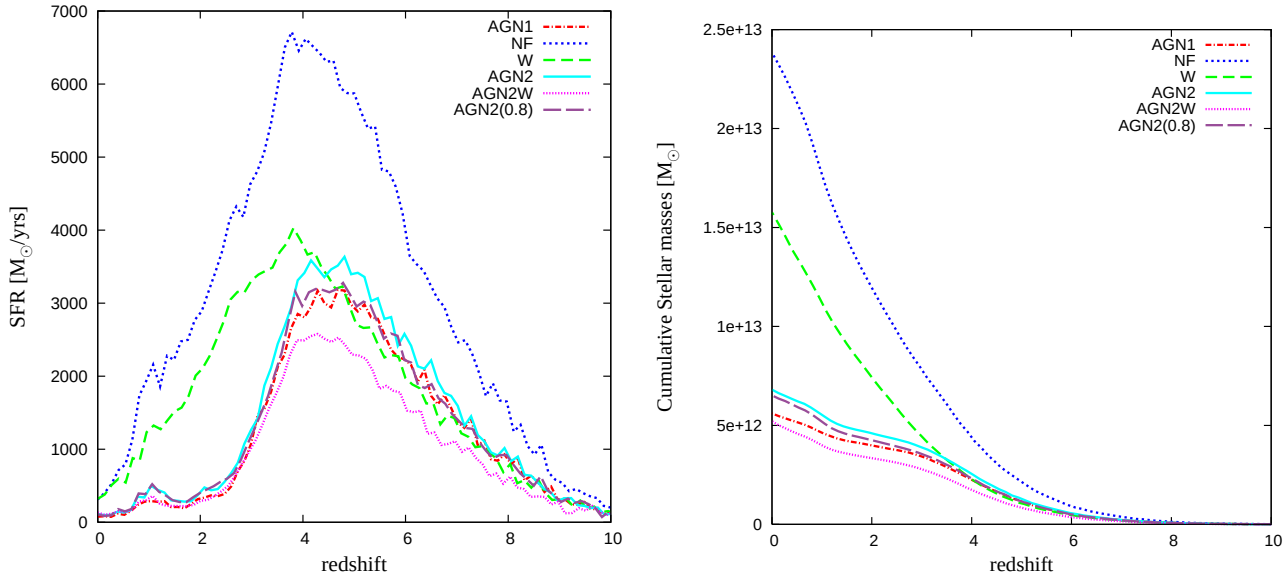

Figure 1. Left panel: the history of star formation rate of the brightest cluster galaxy (BCG) in the g51 cluster for the runs with no feedback (NF, blue short-dashed), with galactic winds (W, green dashed), with standard AGN feedback (AGN1, red dot-dashed) and with modified AGN feedback (AGN2, light-blue solid). Also shown are the results for the AGN2 run with higher radio-mode BH feedback efficiency (AGN2(0.8), purple long-dashed) and for the AGN2 run also including galactic winds (AGN2W, magenta dotted). Right panel: the stellar mass found in the BCG at $z = 0$ that was formed before a given redshift.

adopted a cooling function computed for zero metallicity. Including the contribution of metal lines to the radiative losses increases cooling efficiency and, therefore, gas removal from the hot X–ray emitting phase. However, the price to pay for this reduction of X–ray luminosity is that a far too large baryon fraction is converted into stars within clusters (see below). Quite paradoxically, we also note than including an efficient feedback in the form of galactic winds turns into an increase of X–ray luminosity. This is due to the fact that this feedback prevents a substantial amount of gas from cooling, without displacing it from the central cluster regions, thus increasing the amount of X-ray emitting ICM.

In order to asses the effect of the different resolution used for large and small clusters, we carried out runs of g676 at the same lower resolution of the massive clusters. The results are shown in Fig. 2 with black diamonds connected with arrows to the corresponding higher resolution result. We note that resolution effects go in opposite directions for the NF and W runs. In fact, in the absence of winds, the runaway of cooling with resolution removes from the hot phase a larger amount of gas, thus decreasing X–ray luminosity. On the contrary, higher resolution allows a more accurate description of kinetic feedback, which starts heating gas at higher redshift. As a consequence, radiative losses are compensated at higher resolution for a larger amount of diffuse baryons, which remain in the hot phase, thereby increasing the X–ray luminosity.

As for the runs with AGN feedback, it is quite efficient in decreasing X–ray luminosity at the scale of galaxy groups, thus well recovering the observed L_X–T relation. This conclusion holds for both implementations of the AGN feedback, which have rather small differences. Therefore, although the AGN2 scheme is more efficient in regulating the growth of the central BHs hosted within the BCGs, it has a marginal effect on the X–ray luminosity. These results are in line with those found by Puchwein et al. (2008), who however used the injection of heated bubbles to distribute the energy extracted from the BH accretion. This witnesses that the feedback energy associated to gas accretion onto super-massive BHs is indeed able to produce a realistic L_X–T relation, almost independent of the detail of how the energy is thermalised in the surrounding medium.

3.2 The entropy of the ICM

Entropy level in central regions of clusters and groups is considered another fingerprint of the mechanisms which determine the thermodynamical history of the ICM. Early observational results on the presence of entropy cores (e.g., Ponman et al. 1999) have been more recently revised, in the light of higher quality data from Chandra (e.g., Cavagnolo et al. 2009) and XMM–Newton (e.g., Johnson et al. 2009) observations. These more recent analyses show that entropy level of clusters and groups at R_{500} is higher than predicted by non–radiative simulations, with entropy profiles for relaxed systems continuously decreasing down to the smallest resolved radii (see also Sun et al. 2009).

While radiative simulations of galaxy clusters have been generally shown to reproduce observationalr results at R_{500} (e.g., Nagai et al. 2007; Davé et al. 2008), they generally predict too low entropy levels at smaller radii. For instance, Borgani & Viel (2009) have shown that the entropy at R_{2500} can be reproduced by resorting to a fairly strong pre-heating at $z = 4$. However, this pre-heating must target only relatively overdense regions, to prevent the creation of too large voids in the structure of the Lyman-α forest at $z \sim 2$ (see also Shang et al. 2007).

In the following we use the standard definition of entropy, which is usually adopted in X–ray studies of galaxy clusters (e.g., Sun et al. 2009):

$$K_\Delta = \frac{T_\Delta}{n_{e,\Delta}^{2/3}}, \qquad (3)$$

where T_Δ and $n_{e,\Delta}$ are the values of gas temperature and electron number density computed at R_Δ. As for the temperature, it is computed by following the prescription of spectroscopic like temper-

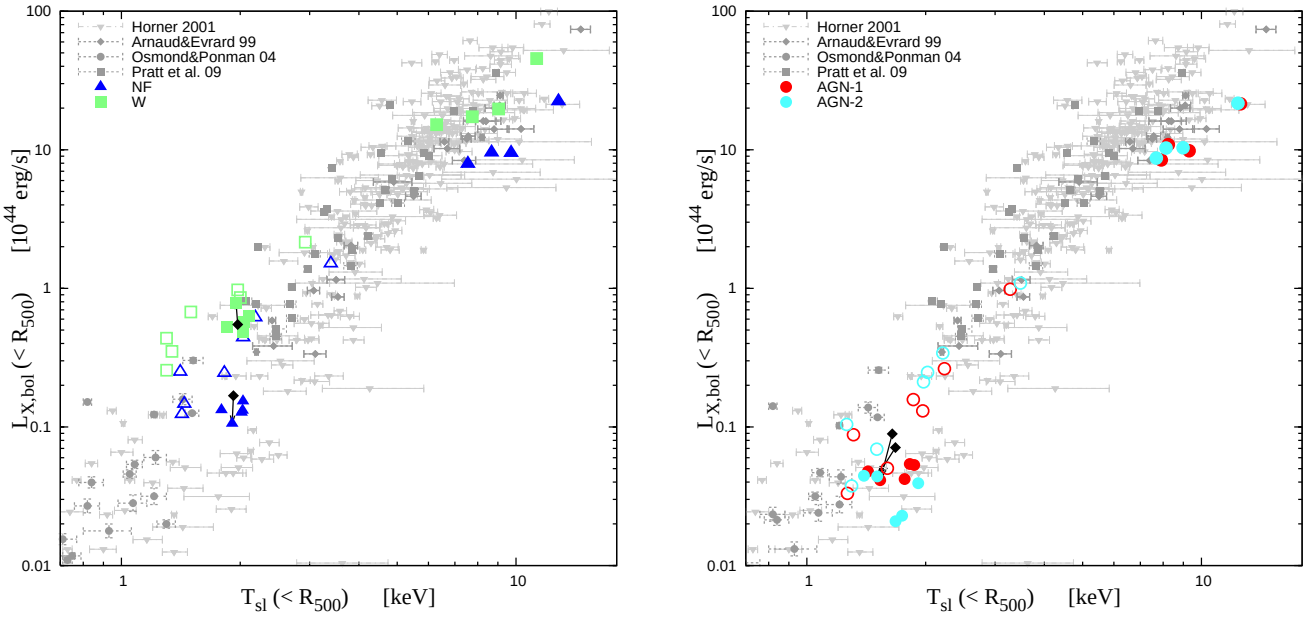

Figure 2. Relation between X–ray luminosity and temperature for simulated (coloured symbols) and observed (grey points with errorbars) clusters and groups. Observational data points are from Arnaud & Evrard (1999) (grey diamonds) and Pratt et al. (2009) (grey squares) for clusters, from Osmond & Ponman (2004) (grey circles) for groups and from Horner (2001) (grey triangles). Data from simulations were computed inside R_{500}. Left panel: results for the no feedback case (NF, blue triangles) and for the case with galactic winds (W, green squares). Right panel: results for the runs with standard AGN feedback (AGN1, red circles) and with the modified AGN feedback scheme, where also a radio-mode regime is included (see text, AGN2; cyan circles). For each series of runs, filled and open symbols refer to the main halo within each resimulated Lagrangian region and to "satellite" halos respectively. Black diamonds refer to the runs at $1\times$ resolution, with arrows pointing to results at $6\times$ higher resolution for the g676 cluster.

ature introduced by Mazzotta et al. (2004). This definition of temperature has been shown to accurately reproduce, within few percents, the actual spectroscopic temperature obtained by fitting spectra of simulated clusters with a single–temperature plasma model, within the typical energy bands where detectors on-board of present X–ray satellites are typically sensitive.

We show in Figure 3 the comparison between our simulations and observational data on groups (Sun et al. 2009) and on clusters (Vikhlinin et al. 2009) for the relation between entropy and temperature at R_{500} and R_{2500} (upper and lower panels, respectively). In order to reproduce the procedure adopted by Sun et al. (2009), we compute the spectroscopic–like temperature of simulated clusters by excluding the core regions within $0.15R_{500}$. As for the runs with no efficient feedback (NF) we note that they produce entropy levels, at both R_{500} and R_{2500}, which are close to the observed ones. This result can be explained in the same way as that found for the L_X–T relation: overcooling, not balanced by an efficient feedback mechanism, removes a large amount of gas from the X–ray emitting phase, while leaving in this hot phase only relatively high entropy gas, which flows in from larger radii as a consequence of lack of central pressure support.

Including winds (W runs) has the effect of increasing the amount of low-entropy gas, which is now allowed to remain in the hot phase despite its formally short cooling time, thanks to the continuous heating provided by winds. As a result, entropy decreases at both radii, for the same reason for which X–ray luminosity increases. As for the runs with AGN feedback, its effect is almost negligible for massive clusters. On the other hand, AGN feedback provides a significant increase of the entropy level in poor systems, an effect which is larger at smaller cluster-centric radii. The resulting entropy is higher than indicated by observational data. Together with the result on the L_X–T relation, this result shows that a rather tuned energy injection is required, which must be able to suppress X–ray luminosity by decreasing gas density, while at the same time reproducing the low entropy level measured at small radii.

3.3 Temperature profiles

A number of comparisons between observed and simulated temperature profiles of galaxy clusters have clearly demomnstrated that a remarkable agreement exists at relatively large radii, $R \gtrsim 0.2R_{180}$, where the effect of cooling is relatively unimportant. While this result, which holds almost independently of the physical processes included in the simulations (e.g., Loken et al. 2002; Borgani et al. 2004; Kay et al. 2007; Pratt et al. 2007; Nagai et al. 2007), should be regarded as a success of cosmological simulations of galaxy clusters, the same simulations have much harder time to predict realistic profiles within cool-core regions (e.g., Borgani et al. 2008, for a recent review). In this regime, radiative simulations systematically produce steep negative temperature profiles, at variance with observations, as a consequence of the lack of pressure support caused by overcooling. This further demonstrates that a suitable feedback mechanisms is required to pressurise the gas, so as to prevent overcooling and turning the temperature gradients from negative to positive in the core regions. While feedback associated to SNe has been proved not to be successful, AGN feedback is generally considered as a likely solution for simulations to produce realistic cool cores. Based on simulations of one relatively low–mass cluster, Sijacki et al. (2008) found that AGN feedback can provide reasonable temperature profiles only if a population of relativistic particles is injected along with thermal energy in inflated bubbles.

We present in Figure 4 the comparison between simulated and

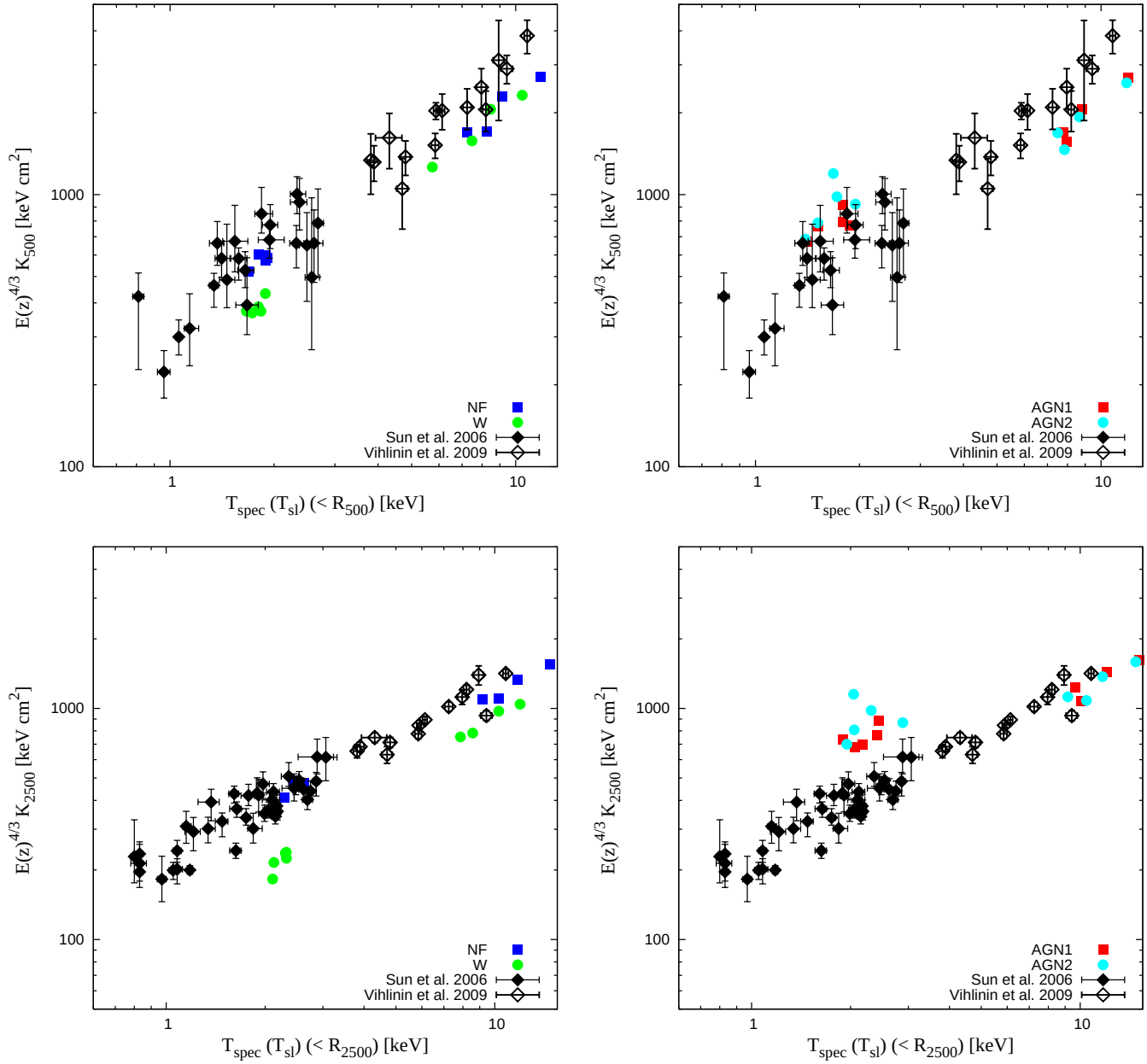

Figure 3. Relation between entropy and temperature for our simulated clusters (coloured circles and squares) and for the observational data points at R_{500} (upper panels) and R_{2500} (lower panels) from Sun et al. (2009) (black filled diamonds) and Vikhlinin et al. (2009) (black open diamonds). Left and right panels show results for the nine central clusters for the runs without (NF: blue squares; W: green circles) and with AGN feedback (AGN1: red squares; AGN2: cyan circles), respectively. For a fair comparison with observations, spectroscopic-like temperatures of the simulated clusters are computed by excluding the regions within $0.15R_{500}$.

observed temperature profiles for galaxy clusters with $T \gtrsim 3$ keV (left panel) and for poorer clusters and groups with $T \lesssim 3$ keV (right panel). Observational results are taken from Leccardi & Molendi (2008b) and Sun et al. (2009) for rich and poor systems, respectively. As for rich clusters, none of the implemented feedback scheme is capable to prevent the temperature spike at small radii, while all models provide a temperature profile quite similar to the observed one at $R \gtrsim 0.3R_{180}$. The situation is different for groups. In this case, both schemes of AGN feedback provide results which go in the right direction. While galactic winds are not able to significantly change the steep negative temperature gradients, the AGN1 and the AGN2 feedback schemes pressurise the ICM in the central regions, thus preventing adiabatic compression in inflowing gas. From the one hand, this result confirms that a feedback scheme not related to star formation goes indeed in the right direction of regulating the thermal properties of the ICM in cool core regions. On the other hand, it also demonstrates that the schemes of AGN feedback implemented in our simulations do an excellent job at the scale of galaxy groups, while they are not efficient enough at the scale of massive clusters.

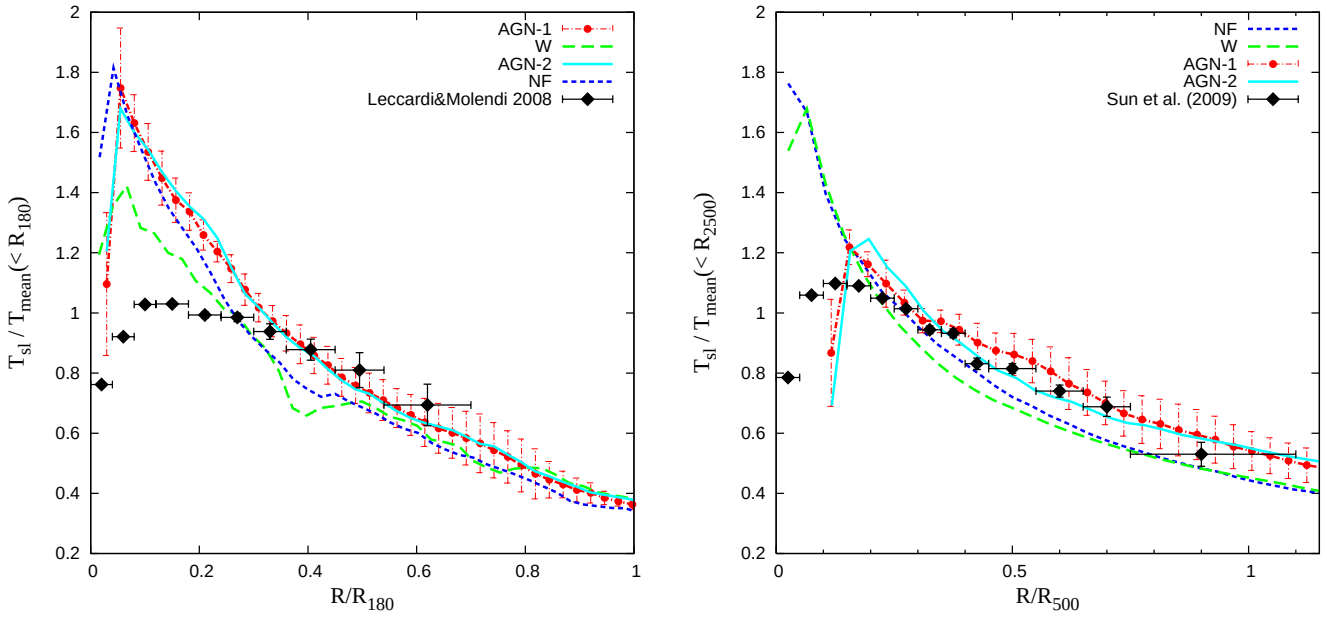

Figure 4. Comparison between the temperature profiles for simulated and observed clusters with $T \gtrsim 3$ keV (left panel) and for groups with $T \lesssim 3$ keV (right panel). In each panel, different lines corresponds to the average simulated profiles computed over the four main massive clusters in the left panel and over the five main low-mass clusters in the right panel, for the different sets of runs: no feedback (NF, blue short dashed), galactic winds (W, green long dashed), standard AGN feedback (AGN1, red dot-dashed), modified AGN feedback (AGN2, cyan solid). For reasons of clarity, we show with errorbars the r.m.s. scatter over the ensemble of simulated clusters only for the AGN1 runs. Observational data points for clusters in the left panel are taken from Leccardi & Molendi (2008b), while those for groups in the right panel are from Sun et al. (2009).

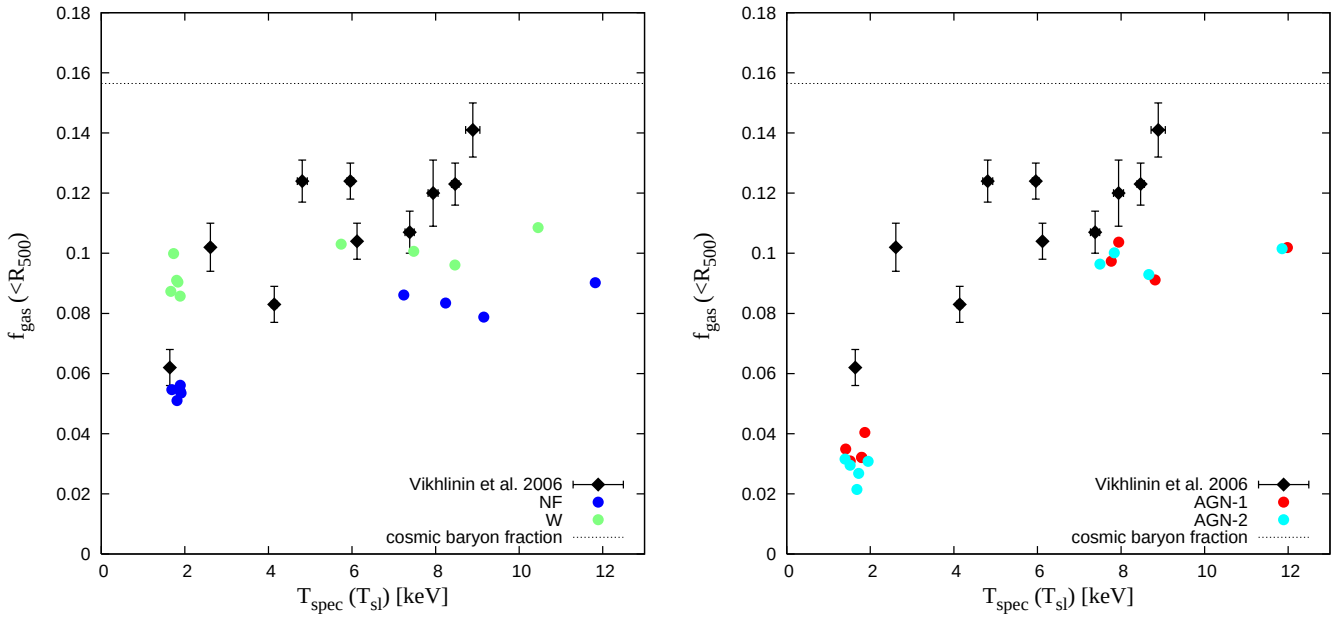

Figure 5. Comparison of the gas fraction within R_{500} in simulations (coloured circles) and observational data from Chandra data (diamonds with errorbars) analysed by Vikhlinin et al. (2006). Left panel: results for the no feedback (NF) runs (dark blue) and for the runs with galactic winds (W, light green). Right panel: results for the runs with the standard AGN feedback (AGN1, dark red) and with modified AGN feedback (AGN2, light cyan). The horizontal dotted line marks the cosmic baryon fraction assumed in the simulations.

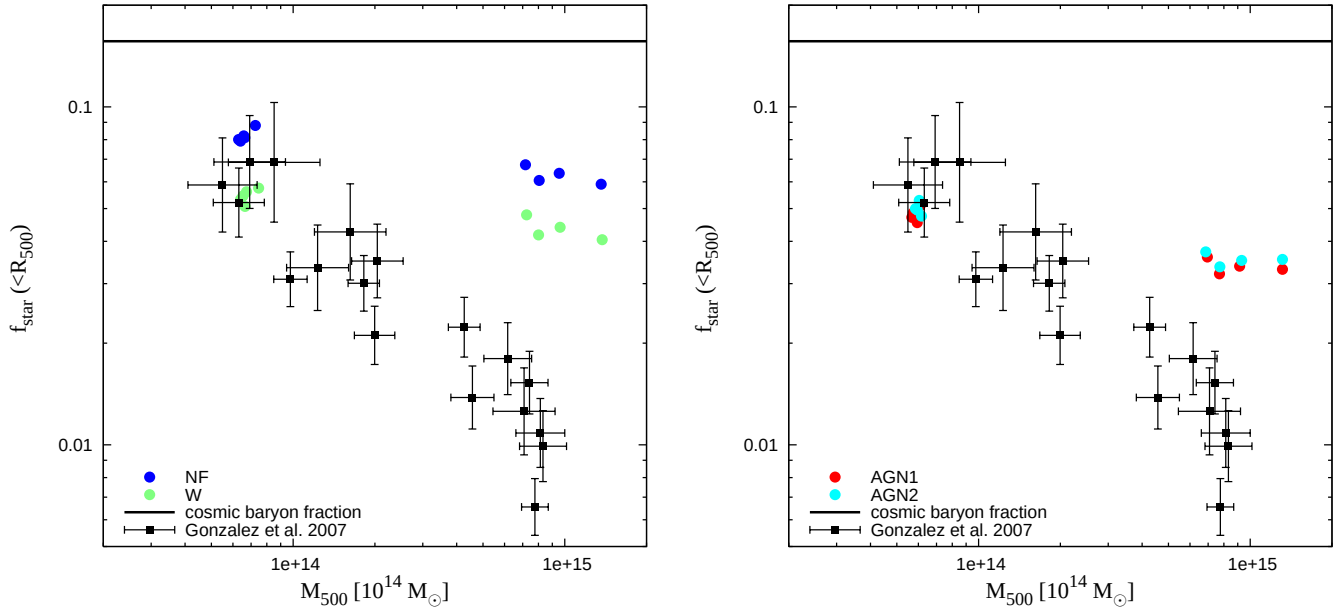

Figure 6. Comparison of the star fraction within R_{500} in simulations (coloured circles) and observations (squares with errorbars). Left panel: results for the no feedback (NF) runs (dark blue) and for the runs with galactic winds (W, light green). Right panel: results for the runs with the standard AGN feedback (AGN1, dark red) and with modified AGN feedback (AGN2, light cyan). Observational points are from Gonzalez et al. (2007) where stellar mass includes the brightest cluster galaxy (BCG), intra-cluster light (ICL) and galaxies within R_{500}.

3.4 The gas and star mass fractions

The inventory of baryons within galaxy clusters represents an important test to understand both the efficiency of star formation and how the gas content is affected by feedback mechanisms. In general, the difficulty of regulating gas cooling in cluster simulations causes a too large stellar mass fraction (e.g., Borgani et al. 2004; Kay et al. 2007; Nagai et al. 2007; Davé et al. 2008), which in turn should correspond to a too low fraction of gas in the diffuse ICM.

We show in Figure 5 the comparison between simulation results and observational data on the mass fraction of hot gas as a function of temperature from Vikhlinin et al. (2006). Gas in simulated clusters is assigned to the hot phase if it is not associated to multi-phase gas particles and if its temperature exceeds 3×10^4K. A comparison between the runs with no feedback (NF) and with galactic winds (W) shows that the latter are characterised in general by larger f_{gas} values. This is in line with the results on the L_X–T relation and confirms that winds are effective in suppressing cooling, thus increasing the hot baryon fraction. While there is a reasonable agreement at the scale of poor clusters, simulations show a weak trend with temperature, with f_{gas} for the hotter systems having values well below the observed ones. As for AGN feedback, it has the effect of increasing f_{gas} for the most massive clusters, although the resulting gas fraction is still below the observational level by about 30 per cent. On the contrary, at the scale of poor clusters the effect of AGN feedback is that of decreasing f_{gas} below the observational limit. Indeed, while in rich systems the effect of AGN feedback is that of reducing overcooling, thereby leaving a larger amount of gas in the hot phase, in poor systems it is so efficient as to displace a large amount of gas outside the cluster potential wells.

Our result on the low value of f_{gas} at the scale of rich clusters, even in the presence of AGN feedback, is in line with the somewhat low value of L_X seen in Fig. 2. However, this result is in disagreement with that presented by Puchwein et al. (2008), who showed instead a good agreement at all temperatures between their simulations including AGN feedback and observational data. There may be two reasons for this difference. Firstly, the scheme to inject AGN-driven high-entropy bubbles used by Puchwein et al. (2008) could provide a more efficient means of stopping cooling in central cluster regions, at the same time preventing excessive gas removal in low-mass systems. Secondly, unlike Puchwein et al. (2008) we include the dependence of metallicity in the cooling function. As already discussed, this significantly enhances cooling efficiency and, therefore, the removal of gas from the hot phase. In order to verify the impact of this effect, we repeated the AGN2 run of g51, by assuming zero metallicity in the computation of the cooling function. As a result, we find that f_{gas} increases from 0.09 to 010. From the one hand, this result implies that the more efficient gas accretion onto BHs, due to metal-cooling, provides a stronger energy feedback which, in turn, balances the higher cooling efficiency. On the other hand, it also implies that the main reason for the difference with respect to Puchwein et al. (2008) should be rather ascribed to the different way in which energy associated to BH accretion is thermalised in the surrounding medium.

As for the behaviour of the mass fraction in stars, we show in Figure 6 the comparison between our simulations and observational results from Gonzalez et al. (2007), who also included in the stellar budget the contribution from diffuse intra-cluster stars (see also Giodini et al. 2009). These results confirm that none of our simulations are able to reproduce the observed decrease of f_{star} with increasing temperature. Overcooling is indeed partially prevented in the presence of winds and, even more, with AGN feedback. However, while simulation results for poor clusters are rather close to observations, overcooling in massive clusters is only partially alleviated by AGN feedback, with values of f_{star} which are larger than the observed ones by a factor 2–3.

In summary, the results presented in this section demonstrated

that AGN feedback has indeed a significant effect in bringing the L_X–T relation and the entropy level of the ICM closer to observational results, while regulating cooling in the central regions. However, the effect is not yet large enough to produce the correct temperature structure in the cool core of massive clusters and, correspondingly, the correct share of baryons between the stellar and the hot gas phase.

4 METAL ENRICHMENT OF THE ICM

The X-ray spectroscopic studies of the content and distribution of metals in the intra-cluster plasma provides important information on the connection between the process of star formation, taking place on small scales within galaxies, and the processes which determine the thermal properties of the ICM. The former affects the quantity of metals that are produced by different stellar populations, while the latter gives us insights on gas-dynamical processes, related both to the gravitational assembly of clusters and to the feedback mechanisms that displace metal-enriched gas from star forming regions.

The detailed model of chemical evolution included in the GADGET-2 code by T07 allows us to follow the production of heavy elements and to study how their distribution is affected by the adopted feedback schemes. The analysis presented in this section is aimed at quantifying the different effects that galactic outflows triggered by SN explosions and AGN feedback have on the enrichment pattern of the ICM. We present results on the Fe distribution and the corresponding abundance profiles, the enrichment age within clusters and groups, the relation between global metallicity and ICM temperature, and the relative abundance of Si with respect to Fe. Results from simulations will be compared to the most recent observational data from the Chandra, XMM-Newton and Suzaku satellites. All the abundance values will be scaled to the the solar abundances provided by Grevesse & Sauval (1998).

To qualitatively appreciate the effect of different feedback mechanisms on the ICM enrichment pattern, we show in Figure 7 the maps of the emission–weighted Fe abundance for the different runs of the g51 massive cluster. Here and in the following, we will rely on emission–weighted estimates of metal abundances. Rasia et al. (2008) have shown that this emission–weighted estimator actually reproduces quite closely the values obtained by fitting the X–ray spectra of simulated clusters, for both Iron and Silicon. As for Oxygen, the emission–weighted estimator has been shown to seriously overestimate the corresponding abundance, especially for hot ($T \gtrsim 3$ keV) systems.

In the run with no AGN feedback (upper panels of Fig.7), we clearly note that including galactic winds produces a level of enrichment which is lower than that in the NF run outside the core region, as a consequence of the lower level of star formation. Therefore, although galactic ejecta are known to be rather efficient in spreading metals in the intergalactic medium at high redshift ($z \gtrsim 2$; e.g., Oppenheimer & Davé 2008; Tescari et al. 2009, Tornatore et al. 2009, in preparation), their effect is not strong enough to compensate the reduction of star formation within cluster regions. In the NF run we note the presence of highly enriched gas clumps which coincide with the halos of galaxies where intense star formation takes place.

A rather different enrichment pattern is provided by AGN feedback (lower panels of Fig.7). Despite the total amount of stars produced in these two runs is smaller than for the run including galactic winds, AGN feedback is highly efficient in spreading metals at high redshift, mostly in correspondence of the peak of BH accretion activity. This demonstrates that AGN feedback provides a rather high level of diffuse enrichment in the outskirts of galaxy clusters and in the inter-galactic medium surrounding them at low redshift.

4.1 Profiles of Iron abundance

We show in Figure 8 the emission-weighted Iron abundance profiles obtained by averaging over the four simulated clusters with $T_{sl} > 3$ keV (left panel) and the five galaxy groups with $T_{sl} < 3$ keV (right panel), compared with observational results. Each panel reports the results for the four adopted feedback schemes. For reasons of clarity we report the 1σ scatter computed over the ensemble of simulated clusters only for the AGN1 runs.

As for rich clusters, simulation predictions are compared with the observational results by Leccardi & Molendi (2008a). These authors analysed about 50 clusters with $T \gtrsim 3$ keV, that were selected from the XMM-Newton archive in the redshift range $0.1 \leqslant z \leqslant 0.3$. After carrying out a detailed modelling of the background emission, they recovered metallicity profiles out to $\simeq 0.4R_{180}$. The results of this analysis show a central peak of Z_{Fe}, followed by a decline out to $0.2R_{180}$, while beyond that radius profiles are consistent with being flat, with $Z_{Fe} \simeq 0.3Z_{Fe,\odot}$ using the solar abundance value by Grevesse & Sauval (1998) ($\simeq 0.2$ in units of the solar abundance by Anders & Grevesse (1989), as reported by Leccardi & Molendi 2008a).

All our simulations predict the presence of abundance gradients in the central regions, whose shape is in reasonable agreement with the observed one, at least for $R \lesssim 0.1R_{180}$. The lowest enrichment level is actually found for the NF run, despite the fact that this model produces the most massive BCGs. The reason for this lies in the highly efficient cooling that selectively removes the most enriched gas, which has the shortest cooling time, thus leaving metal poorer gas in the diffuse phase. Runs with galactic winds (W) and AGN feedback (AGN1 and AGN2) are instead able to better regulate gas cooling in central region, thus allowing more metal-rich gas to survive in the hot phase. For this reason, W and AGN runs predict profiles of $Z_{\rm Fe}$ which are steeper than for the NF runs in the central regions, $\lesssim 0.1R_{180}$. Quite interestingly, the effect that different feedback mechanisms have in displacing enriched gas and regulating star formation almost balance each other in the central cluster regions, thus producing similar profiles. However, the different nature of SN-powered winds and AGN feedback leaves a clear imprint at larger radii.

As for the runs with no feedback (NF), they produce a rather high level of enrichment out to $\sim 0.3R_{180}$, while rapidly declining at larger radii. In this model, the high level of star formation provides a strong enrichment of the gas in the halo of galaxies which will merge in the clusters. During merging, this gas is ram–pressure stripped, thus contributing to enhance the enrichment level of the ICM. The situation is different for the runs with winds. As already mentioned, galactic outflows are efficient in displacing gas from galactic halos at relatively high redshift, $z \gtrsim 2$, when they provide an important contribution to the enrichment of the intergalactic medium (IGM; e.g., Oppenheimer & Davé 2008). At the same time, this feedback is not efficient to quench cooling of enriched gas at low redshift. As a consequence, no much enriched gas is left to be stripped by the hot cluster atmosphere from the halos of merging galaxies, thus explaining the lower enrichment level beyond $0.1R_{180}$.

As for the runs with AGN feedback, they produce a shape on

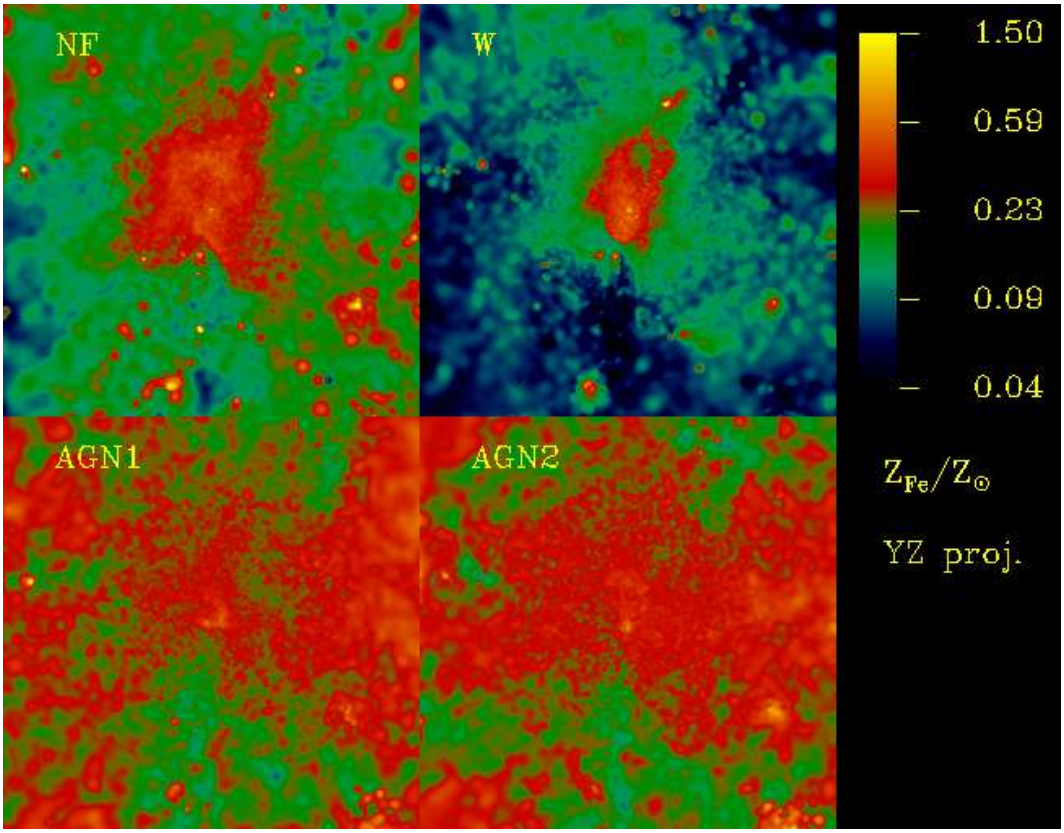

Figure 7. Maps of emission weighted Fe abundance in the g51 cluster for the runs without feedback (NF, top left), with winds (W, top right) and with AGNs (AGN1 and AGN2, bottom left and bottom right, respectively). Each map has a side of $2R_{vir}$. Abundance values are expressed in units of the solar value, as reported by Grevesse & Sauval (1998), with color coding specified in the right bar.

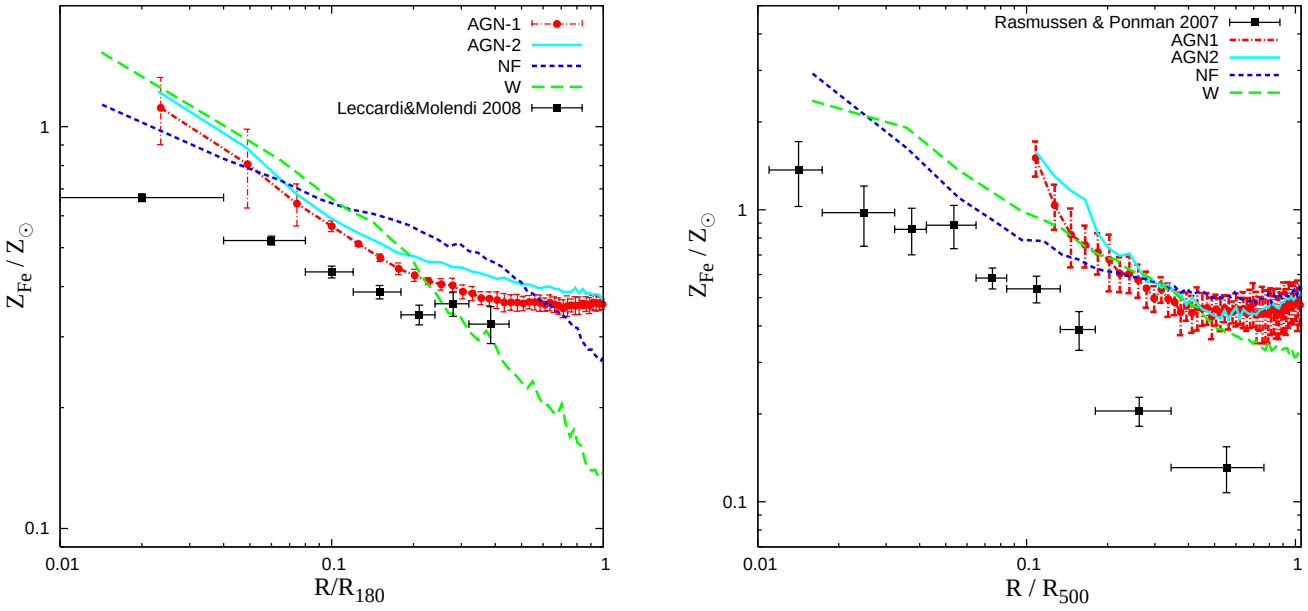

Figure 8. Comparison between the observed and the simulated profiles of emission-weighted Iron metallicity. Left panel: average $Z_{\rm Fe}$ profiles for galaxy clusters with $T_{500} > 3$ keV. Observational data points are taken from Leccardi & Molendi (2008a). Right panel: average $Z_{\rm Fe}$ profiles for the five simulated galaxy groups with $T_{500} < 3$ keV. Observational data points are taken from Rasmussen & Ponman (2007). In both panels different lines correspond to the average profiles computed for the different runs: no feedback (NF, blue short dashed), galactic winds (W, green long dashed), standard AGN feedback (AGN1, red dot-dashed), modified AGN feedback (AGN2, cyan solid). For reasons of clarity, we show with 1σ errorbars over the ensemble of simulated clusters only for the AGN1 runs.

the abundance profiles quite close to the observed ones, with a flattening beyond $\simeq 0.2R_{180}$. In this case, the effect of AGN feedback is that of displacing large amounts of enriched gas from star forming regions at high redshift (see also Bhattacharya et al. 2008) and, at the same time, to efficiently suppress cooling at low redshift. The fact that the level of Z_{Fe} is almost constant out to R_{180} and beyond, witnesses that the main mechanism responsible for enrichment in this case is not ram–pressure stripping, whose efficiency should decline with cluster-centric radius. Instead, enrichment is this case is dominated by the diffuse accretion of pre-enriched IGM. We note that the AGN2 scheme tends to predict slightly higher Z_{Fe} values that AGN1. This is due to the effect of the more efficient radio-mode feedback, included in the former scheme, which provides a more efficient removal of gas from the halos of massive galaxies.

Although models with AGN feedback produce the correct shape of the Iron abundance profiles, their normalisation is generally higher than for the observed ones. This overproduction of Iron could be due to the uncertain knowledge of a number of ingredients entering in the chemical evolution model implemented in the simulation code. For instance, differences between different sets of stellar yields turn into significant differences in the resulting enrichment level (e.g., Tornatore et al. 2007; Wiersma et al. 2009). Furthermore, a reduction of the Iron abundance can also be achieved by decreasing the fraction of binary systems, which are the progenitors of SNe-Ia (e.g., Fabjan et al. 2008). For these reasons, we believe that the shape of the abundance profiles, instead of their amplitude, should be considered as the relevant observational information to be used to study the impact that different feedback mechanisms have on the ICM enrichment pattern.

In the right panel of Fig. 8 we compare the average $Z_{\rm Fe}$ profiles of the five simulated galaxy groups with observational results from the analysis of 15 nearby galaxy groups observed with Chandra (Rasmussen & Ponman 2007). Also in this case, the profiles from simulations have a slope quite similar to the observed one out to $R \simeq 0.3R_{500}$, although with a higher normalisation. At larger radii, the effect of AGN feedback is again that of providing rather flat profiles. This result is at variance with the observed profiles in the outermost radii. Indeed, differently from rich clusters, galaxy groups apparently show a negative gradient of Iron abundance out to the largest radii covered by observations, with no evidence of flattening. This result further demonstrates the relevance of pushing observational determinations of the ICM enrichment out to the large radii, which it is mostly sensitive to the nature of the feedback mechanism. If confirmed by future observations, this result may indicate that AGN feedback needs to be mitigated at the scale of galaxy groups, for it not to displace too large amounts of enriched gas.

As pointed out by Rebusco et al. (2005), the central Z_{Fe} peak in cool-core (CC) clusters (see also De Grandi et al. 2004) should be closely related to the star (light) distribution of the BCG. On the other hand, differences between the stellar mass profile and the metal abundance profile should be the signature of dynamic processes which mix and transport metals outside the BCG. In this way, Rebusco et al. (2005) derived the amount of diffusion, to be ascribed to stochastic gas motions, which is required to explain the shallower profiles of Z_{Fe} with respect to the BCG luminosity profiles. Roediger et al. (2007) carried out simulations of isolated cluster–sized halos in which bubbles of high-entropy gas are injected to mimic the effect of AGN feedback. They showed that the gas diffusion associated to the buoyancy of such bubbles is indeed able to considerably soften an initially steep metallicity profile.

In order to verify to what extent gas dynamical processes, associated either to the hierarchical cluster build-up or to feedback energy release, are able to diffuse metals, we compare in Figure 9 the average $Z_{\rm Fe}$ profiles and the stellar mass profiles for the massive clusters. As for the NF and W runs, we clearly see a central peak in the stellar mass density profile, related to the BCG, followed by a more gentle decline, which traces a diffuse halo of intracluster stars surrounding the BCG (e.g., Murante et al. 2007). Quite clearly, the $Z_{\rm Fe}$ profiles are flatter than the distribution of stars at $R \lesssim 0.1R_{vir}$. Since no feedback processes are at work in the NF runs, the flatter $Z_{\rm Fe}$ profile is due to the effect of selective cooling of highly enriched gas, rather than to stochastic gas motions. The same argument can be applied also to the runs including galactic winds (W), for which the kinetic energy provided galactic ejecta is not enough to fully regulate star formation in central cluster regions (see also Fig. 5). At intermediate radii, $R \simeq (0.1-0.5)R_{vir}$, profiles of Iron abundance and stellar mass have quite similar slopes in both the NF and W runs. At even larger radii, instead, the $Z_{\rm Fe}$ profile becomes again shallower than the stellar mass profile, a trend which persists even beyond the virial radius. At such large radii the shallower slope of $Z_{\rm Fe}$ can not be explained by the effect of gas cooling. It is rather due to the effect of gas dynamical processes which help mixing the enriched gas.

As for AGN feedback, its effect is instead that of providing a similar slope for $Z_{\rm Fe}$ and stellar mass profiles at $R \lesssim 0.2R_{vir}$. This similarity is due to two concurrent effects. The first one is the suppression of star formation, which allows now central enriched gas to be pressurised by the AGN feedback, so as to leave a relatively larger amount of metal-enriched gas in the hot phase. The second one is the shape of the stellar mass profile, which is less concentrated in the presence of AGN feedback. While the two profiles are similar in the central regions, the $Z_{\rm Fe}$ profile is instead much shallower at larger radii, $R \gtrsim 0.3R_{vir}$. Even an efficient AGN feedback can not be able to displace at low redshift significant amounts of enriched gas from the central regions of massive clusters beyond R_{vir}. Therefore, the flatter abundance profiles in the outskirts of rich clusters can only be justified by the action played by AGN feedback at high redshift. In fact, at $Z \gtrsim 2$ AGN efficiently removed enriched gas from galaxies and quenched star formation, thus preventing metals from being locked back in the stellar phase.

4.2 When was the ICM enriched?

In this section we discuss how the different feedback mechanisms change the cosmic epoch at which ICM was enriched. To this purpose, we define the average age of enrichment of a gas particle at redshift z as

$$\bar{t}(z) \, = \, \frac{\sum_i \Delta m_{Z,i} t_i}{m_Z(z)} \, , \qquad (4)$$

where the sum is taken over all time-steps performed by the simulation until redshift z, $\Delta m_{Z,i}$ is the mass in metals received by the particle at the i-th time-step, t_i is the cosmic time of that time-step and $m_Z(z)$ is the total metal mass received by the particle before z. According to this definition, a large value of enrichment age, at a given redshift, corresponds to more recent enrichment, while smaller values of $\bar{t}(z)$ indicate more pristine enrichment. In the limit in which all the metals are received by a particle at the considered redshift z, then the enrichment age coincides with the cosmic age at z. Once computed for each gas particle, we then compute the mass-weighted mean of these ages of enrichment taken over all the particles having non–vanishing metallicity.

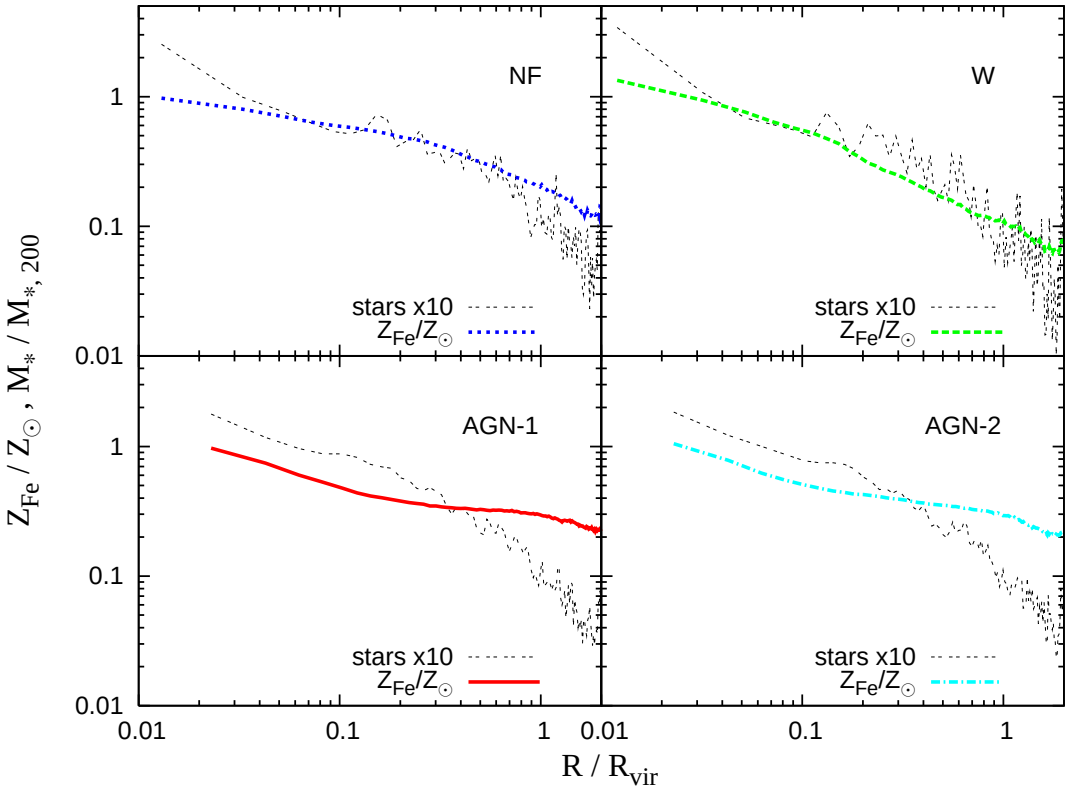

Figure 9. Comparison between the stellar mass density profiles, normalised to the corresponding value computed within R_{200} (black short dashed lines), and the Iron abundance profiles (coloured lines). For reasons of clarity stellar profiles are shifted by a factor 10. All curves refer to the average profiles computed over the four massive clusters. From top left to bottom right panels we show results for the runs with no feedback (NF, blue short dashed), with galactic winds (W, green long dashed), with standard AGN feedback (AGN1, red solid) and modified AGN feedback (AGN2, cyan dot-dashed).

Figure 10 shows how the enrichment age of the ICM changes with the cluster-centric distance for the different feedback models, for both rich clusters (top panel) and for poor clusters (bottom panel). In all cases, we note a decline towards small radii, although with different slopes. This demonstrates that gas in central regions has been generally enriched more recently than in the outskirts. In the innermost regions, the typical age of enrichment correspond to a look-back time of about 2–3 Gyr, while increasing to 5–8 Gyr around the virial radius. This confirms that metal enrichment in the central cluster regions receives a relatively larger contribution by star formation taking place in the BCG, and by stripping of enriched gas from infalling galaxies, whose star formation has been "strangulated" only recently by the action of the hot cluster atmosphere. On the contrary, enrichment in the outskirts has a relatively larger contribution from high–z star formation, which provides a more widespread IGM enrichment.

As for massive clusters, we note that the effect of galactic winds (W runs) is that of providing an earlier enrichment with respect to the model with no efficient feedback (NF runs), with a difference of about 1 Gyr, at all radii. This is quite expected, owing to the efficient action that winds play in displacing metals from star forming regions at high redshift. The difference between W and NF runs is larger for the less massive clusters, consistent with the expectation that winds are more efficient in transporting metals outside shallower potential wells.

Quite interestingly, AGN feedback provides a steeper radial dependence of the enrichment age, with rather similar results for the two alternative schemes of implementation (AGN1 and AGN2). In the central regions it is comparable to that of the NF runs, while becoming larger than that of the W runs for $R \gtrsim 0.3 R_{vir}$ ($\gtrsim 0.6 R_{vir}$) for rich (poor) clusters. The relatively recent enrichment age in central regions may look like a paradox, owing to the effect that AGN feedback has in suppressing low redshift star formation within the BCG (see Fig.1). However, we should remind that an aside effect of suppressing star formation is also that of preventing recently enriched gas from being locked back in stars. Therefore, although metal production in central regions is suppressed in the presence of AGN feedback, this effect is compensated by the suppression of cooling of recently enriched gas. The effect of AGN feedback in providing a more pristine metal enrichment becomes apparent in the outskirts of clusters. Indeed, the IGM in these regions has been efficiently enriched at high redshift, $z \simeq 3$–4, when BH accretion reached its maximum activity level and displaced enriched gas from star forming galaxies. After this epoch, little enrichment took place as a consequence of the rapidly declining star formation, thus justifying the older enrichment age. Consistently with this picture, we also note that the increase of enrichment age with radius is more apparent for poorer clusters, where AGN feedback acted in a more efficient way.

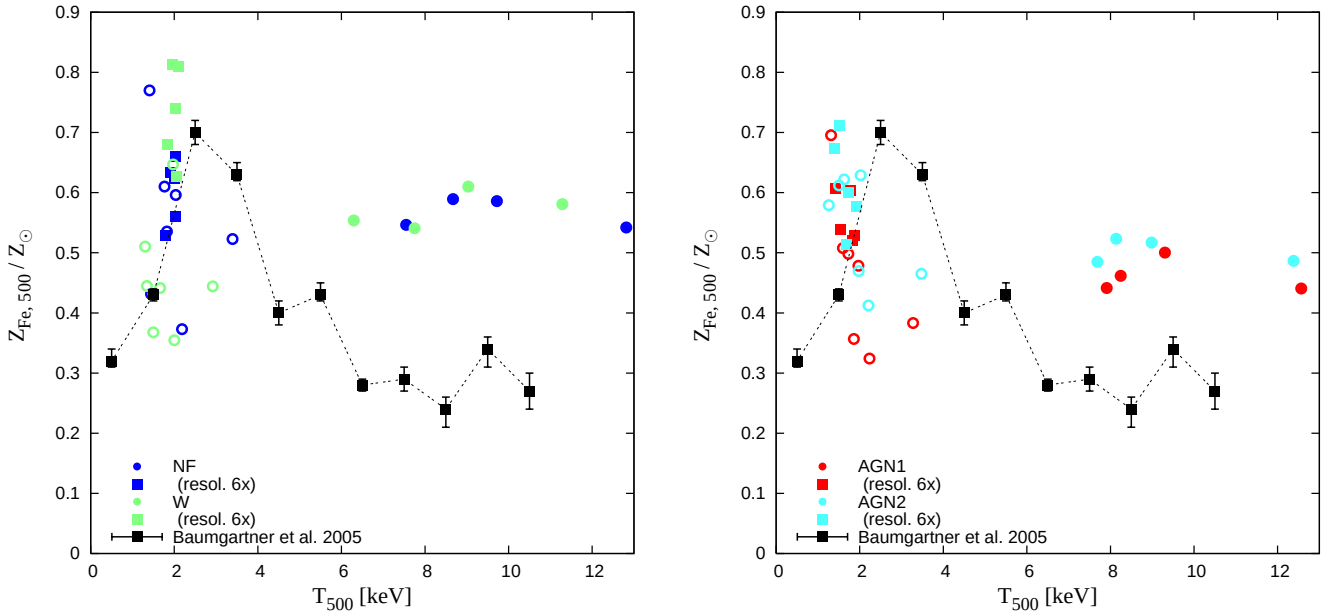

Figure 11. Comparison between observed (solid squares with errorbars) and simulated (coloured symbols) relation between global Iron abundance and temperature. The left panel shows the results for the NF (dark blue) and W (light green) runs, while the right panel shows the results for the AGN1 (dark red) and AGN2 (light cyan) runs. In all cases, filled and open circles refer to the main halos of the resimulated Lagrangian regions with massive clusters and to the satellites, respectively. The main-halo galaxy groups are instead plotted with filled squares. Emission–weighted Iron abundance and spectroscopic–like temperature for simulations are both computed within R_{500}. Observational results refer to the sample of clusters observed with ASCA and analysed by Baumgartner et al. (2005).

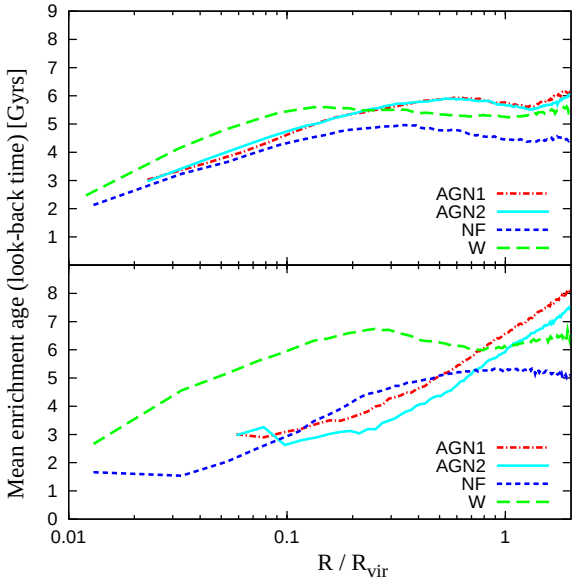

Figure 10. Average age of enrichment as a function of the cluster-centric distance. The y-axis is for the look-back time at which the ICM was enriched (in Gyr). The top panel is for the four massive clusters with $M_{200} > 10^{15}\,h^{-1}M_\odot$, while the bottom panel is for the five galaxy groups with $M_{200} \simeq 10^{14}\,h^{-1}M_\odot$. Different lines corresponds to the average age of enrichment computed within the set of simulated cluster: no feedback (NF, short dashed), galactic winds (W, long dashed), standard AGN feedback (AGN1, dot-dashed), modified AGN feedback (AGN2, solid).

4.3 The metallicity - temperature relation

In Figure 11 we present results on the abundance of Iron as a function of cluster temperature, by comparing simulation results for the different feedback schemes with observational results from the analysis of the ASCA Cluster Catalogue (ACC; Horner 2001) carried out by Baumgartner et al. (2005). Due to the relatively poor angular resolution of the ASCA satellite, the extraction region for each cluster was selected to contain as much flux as possible. Since a unique extraction radius is not defined for the observed catalogue, we adopt R_{500} as a common extraction radius to compute Iron abundances and temperatures of simulated clusters. We verified that adopting instead a larger extraction radius (e.g. R_{vir}) slightly lowers the spectroscopic-like temperatures without changing substantially the results on $Z_{\rm Fe}$. In their analysis, Baumgartner et al. (2005) partitioned their large sample of clusters in temperature bins. Then, a global value of $Z_{\rm Fe}$ was computed by combining all the clusters belonging to the same temperature bin. In this way, errorbars associated to the observational data points shown in Fig. 11 only account for the statistical uncertainties in the spectral fitting procedure after combining all clusters belonging to the same temperature bin, while they do not include any intrinsic scatter (i.e., cluster-by-cluster variation) in the $Z_{\rm Fe}$ –T relation. This has to be taken in mind when comparing them to simulation results, for which we did not make any binning in temperature.

In both panels we see that simulations of hot ($T > 6$ keV) systems produce values of $Z_{\rm Fe}$ which are above the enrichment level found in observations, $\sim 0.3Z_\odot$. This result is consistent with the fact that $Z_{\rm Fe}$ profiles for simulated clusters have a larger normalisation than the observed ones (see Fig. 8). NF and W runs predict $Z_{Fe} \simeq (0.5-0.6)Z_{Fe,\odot}$, with a slightly lower value, $Z_{Fe} \simeq (0.4-0.5)Z_{Fe,\odot}$ for the runs with AGN feedback.

As for the simulations of the poorer systems, with $T \simeq (1-3)$ keV, they have instead a larger scatter. This indicates more diversity in the impact that gas-dynamical and feedback processes have in determining the enrichment pattern within smaller systems. The effect of AGN feedback for these systems is that of decreasing the value of $Z_{\rm Fe}$ by about $0.1 Z_{Fe,\odot}$. The rather large spread of abundance values and the limited number of simulated systems do not allow to establish whether simulations reproduce the increase of $Z_{\rm Fe}$ with ICM temperature for systems in the range $T \simeq (1-3)$ keV.

Observations suggests that $Z_{\rm Fe}$ is almost independent of temperature above 6 keV, a trend which is in fact reproduced by simulation results. However, between 3 and 6 keV observed clusters show a drop in metallicity by about a factor two. Although simulations predict somewhat higher metallicity values at low temperatures, still it is not clear whether they reproduce the decrease, by more than a factor 2, suggested by observations. A potential complications in comparing observational and simulation results for systems with $T \sim 3$ keV is that the spectroscopic value of $Z_{\rm Fe}$ for these systems is contributed by both K and L lines. As originally noted by Buote (2000) in the analysis of ASCA data, fitting with a single-temperature model a plasma characterised by a multi-temperature structure, with the colder component below 1 keV, leads to an underestimate of the Iron abundance (the so-called iron-bias; see also Molendi & Gastaldello 2001; Buote et al. 2003). In this case, a simple emission–weighted definition of $Z_{\rm Fe}$ from simulations may not be fully adequate. A correct procedure would require extracting a mock X–ray spectrum from simulated clusters, to be fitted with a multi–temperature (and multi–metallicity) plasma model (e.g., Rasia et al. 2008). Finally, one should also note that more recent determinations of the $Z_{\rm Fe}$–T relation from XMM–Newton data, although based on a much smaller number of clusters, suggests a less pronounced decrease for systems hotter than 3 keV (e.g., Werner et al. 2008). There is no doubt that a systematic analysis of nearby clusters within the Chandra and XMM-Newton archives would help to confirm or disprove the metallicity–temperature relation based on ASCA observations.

4.4 The $Z_{\rm Si}/Z_{\rm Fe}$ relative abundance

The relative abundance of elements produced in different proportions by different SN types is directly related to the shape and possible evolution of the initial mass function. Furthermore, studying how relative abundances change with cluster-centric distance provides insights on the different timing of enrichment and on how different metals, produced over different time-scales, are mixed by gas-dynamical processes. ASCA data analysed by Loewenstein & Mushotzky (1996), Fukazawa et al. (1998) and Finoguenov et al. (2000) originally suggested that cluster outskirts are predominantly enriched by SNe-II. A similar result was found more recently also by Rasmussen & Ponman (2007), who analysed XMM data for poor clusters with $T \lesssim 3$ keV. On the other hand, Suzaku observations of low temperature clusters and groups (Sato et al. 2008, 2009a, 2009b) show instead a rather flat profile of Z_{Si}/Z_{Fe} out to large radii, $\simeq 0.3 R_{vir}$, thus implying that SNe-Ia and SNe-II should contribute in similar proportions to the enrichment at different radii.

In this section, we focus our attention on the $Z_{\rm Si}/Z_{\rm Fe}$ ratio for low temperature clusters. We show in Figure 12 the emission-weighted map of the $Z_{\rm Si}/Z_{\rm Fe}$ ratio for the four different feedback schemes applied to the g676 cluster. For the run with no feedback (NF), we note that $Z_{\rm Si}/Z_{\rm Fe}$ is generally quite patchy. It reaches higher values in correspondence of high–density star forming regions, a feature which is also shared in different proportions by the other runs. Indeed, the products of SNe-II are released over a short time scale, since they are synthesised by massive stars. As a result, their distribution tends to trace preferentially the distribution of star-forming regions. On the other hand, SNe-Ia release metals over a longer time-scale. In fact, these stars have time to leave star forming regions, as a consequence of the same dynamical effects which generate a population of inter-galactic stars (e.g., Murante et al. 2007; Zibetti et al. 2005), thereby providing a more widespread enrichment pattern. Therefore, our simulations predict that diffuse intra-cluster stars provide a significant contribution to the enrichment of the intra-cluster medium (see also Tornatore et al. 2007).

A comparison of the maps for the NF and W runs shows that they have comparable levels of $Z_{\rm Si}/Z_{\rm Fe}$ within the central regions. In these regions we expect that ram–pressure stripping is the dominant process in removing gas from merging galaxies (see also Kapferer et al. 2007) and, therefore, in efficiently mixing in the ICM the nucleosynthetic products of different stellar populations. On the contrary, in the cluster outskirts winds have been much more efficient in removing freshly produced metals from galaxies during the cluster assembly, therefore providing a relatively more widespread Si distribution, with respect to the NF case in which no galactic outflows are included.

The runs with AGN feedback exhibit a behaviour in the cluster outskirts which is qualitatively similar to that of the W run, although with slightly higher values of $Z_{\rm Si}/Z_{\rm Fe}$. This indicates that AGN feedback has a higher efficiency in mixing SN-Ia and SN-II products. As for the central regions, the truncation of recent star formation by AGN feedback would lead to the naive expectation that a relatively higher value of Iron abundance with respect to Silicon should be found. The results shown in the bottom panels of Fig.12 lead in fact to the opposite conclusion, with a marked increase of $Z_{\rm Si}/Z_{\rm Fe}$ in the core regions. The reason for this lies again in the effect of selective removal of metal-enriched gas associated to cooling. Total metallicity of the gas around the BCG is dominated by SNe-II products. Therefore, gas more enriched by SNe-II has a relatively shorter cooling time. As a consequence, suppression of cooling in the core regions by AGN feedback tends to increase the amount of SN-II products in the ICM, thereby justifying the increase of $Z_{\rm Si}/Z_{\rm Fe}$ with respect to the runs not including AGN.

This qualitative picture is also confirmed by the profiles of $Z_{\rm Si}/Z_{\rm Fe}$, that are plotted in Figure 13. In each panel, simulation results show the average profile, computed over the 5 main relatively poor clusters, for each feedback model. In the left panel simulation results are compared with observational results by Rasmussen & Ponman (2007) from the analysis of 15 nearby galaxy groups observed with Chandra. Also shown with the two horizontal lines are the values of $Z_{\rm Si}/Z_{\rm Fe}$ produced by SNe-Ia and SNe-II for a simple stellar population of initial solar metallicity, having a Salpeter IMF, using the same sets of yields adopted in our simulations.

Observational data show a rather flat profile of $Z_{\rm Si}/Z_{\rm Fe}$ with a value close to solar at small radii, followed by a sudden increase beyond $\simeq 0.2 R_{500}$. Taken at face value, this result would imply that at $\sim 0.5 R_{500}$ the enrichment is mostly contributed by SNe-II, while a mix of different stellar populations is required in the cluster centre. Although this result is qualitatively similar to that suggested by the visual inspection of the $Z_{\rm Si}/Z_{\rm Fe}$ maps of Fig.12, simulation results are quantitatively different from those by Rasmussen & Ponman (2007). Indeed, in no case simulations predict an increase of Z_{Si}/Z_{Fe} beyond $0.2 R_{500}$. While the maps sug-

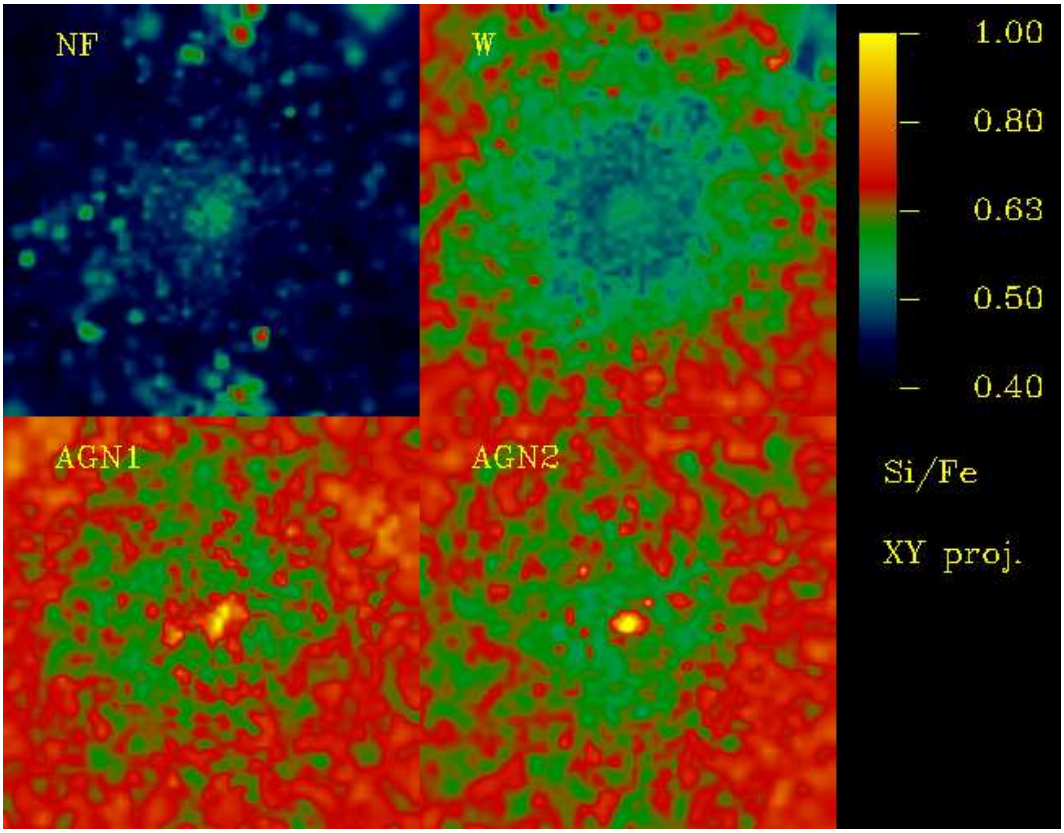

Figure 12. Maps of the emission–weighted $Z_{\rm Si}/Z_{\rm Fe}$ distribution for the runs of the g676 cluster without feedback (NF, top left), with winds (W, top right), with AGNs (AGN1 and AGN2, bottom left and right, respectively). The side of each map is $2R_{vir}$. Abundance values are expressed in units of the solar value, as reported by Grevesse & Sauval (1998), with color coding specified in the right bar.

gest that such an increase is also expected in simulations, it takes place only for $R > R_{500}$, with the largest values reaching at most the solar one. Within the radial range covered by Chandra observations, both NF and W runs show rather flat profiles. Also in this case, we are more interested in the slope of the $Z_{\rm Si}/Z_{\rm Fe}$ profile, rather than in its normalisation. Indeed, too low values of Z_{Si}/Z_{Fe} in simulations by about 0.3 (in solar units) can be be either due to the choice of the IMF or to adopted stellar yields.

As for the runs with AGN feedback the profiles of Z_{Si}/Z_{Fe} confirm the expectation gained from the maps of Fig.12 for a relative increase of the Si abundance in the central regions. As for the behaviour at large radii, $R \gtrsim 0.2R_{500}$, also AGN feedback does not predict the pronounced increase see in the Chandra data by Rasmussen & Ponman (2007).

As already mentioned, this observational evidence for an enhancement of SN-II products in the outskirts of groups is not confirmed by Suzaku data (Sato et al. 2008, 2009a,2009b) and XMM-Newton (Silvano Molendi, private communication). As shown in the left panel of Fig.12, Suzaku observations of Abell 262, NGC 507 and AWM 7 indicate a profile of $Z_{\rm Si}/Z_{\rm Fe}$ which is consistent with being flat out to $0.3R_{vir}$ (corresponding to about $0.5R_{500}$). While it is not the purpose of this work to address the reason for the different results coming from different satellites, we want to stress the great relevance of tracing the pattern of ICM enrichment out to the largest possible radii. Indeed, this is the regime where gas-dynamical processes related to the cosmological build-up of clusters, past history of star formation and nature of feedback processes regulating star formation, all play a role in determining the distribution of metals.

In summary, the analysis of chemical enrichment in our simulations of galaxy clusters confirms that the resulting metallicity distribution in the ICM is given by the interplay between gas cooling, which tends to preferentially remove more enriched gas from the hot phase, feedback processes, which displace gas from star forming regions and regulate star formation, and gas dynamical processes associated to the hierarchical build-up of galaxy clusters. In particular, feedback implemented through the action of galactic winds powered by SN explosions or through energy extracted from gas accretion onto super-massive BHs, leave distinct features on the resulting pattern and timing of ICM enrichment.

5 CONCLUSIONS

We presented the analysis of an extended set of cosmological hydrodynamical simulations of galaxy clusters aimed at studying the different effects that stellar and AGN feedback have on the thermal and chemo-dynamical properties of the intra-cluster medium (ICM). Using a version of the Tree-SPH GADGET-2 code (Springel 2005), which also includes a detailed description of chemical enrichment (Tornatore et al. 2007), we carried out simulations of 16 clusters identified within 9 Lagrangian regions extracted from a lower-resolution parent cosmological box (Dolag et al. 2008). All cluster simulations of this set have been run using different prescriptions for the feedback: without including any efficient feed-

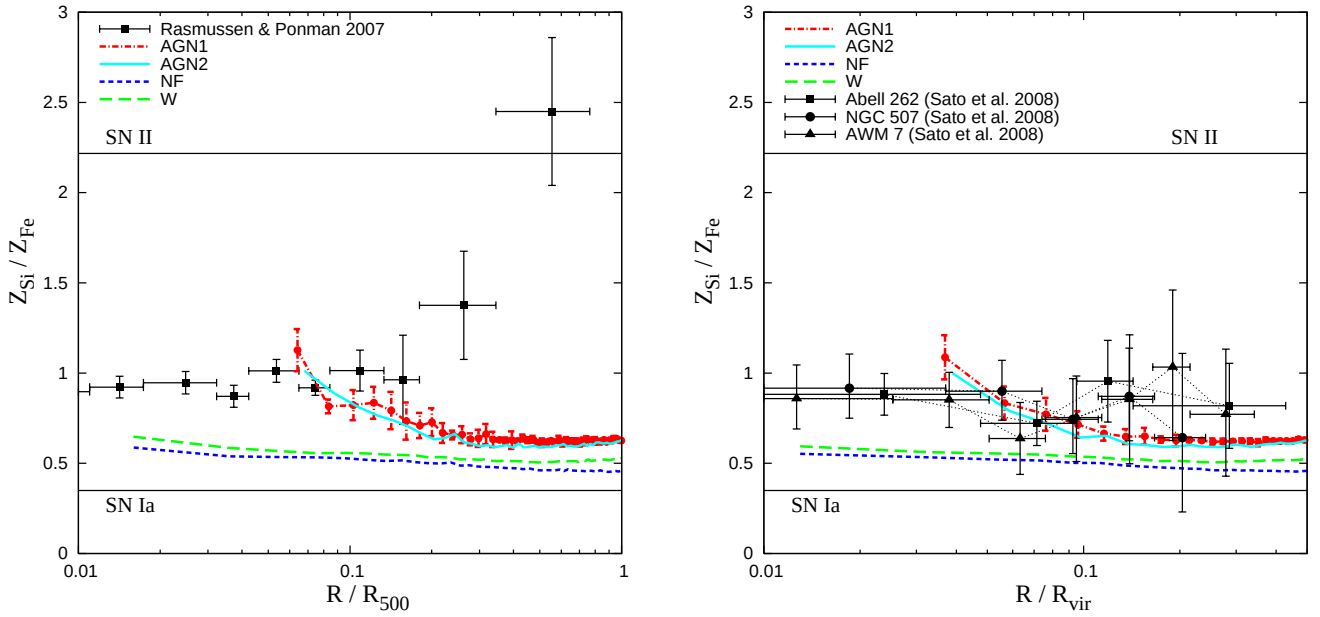

Figure 13. Comparison between observed and the simulated profiles of Silicon abundance relative to Iron, $Z_{\rm Si}/Z_{\rm Fe}$. In each panel, different lines correspond to the average profiles computed over clusters having $T_{500} < 3$ keV for the different sets of runs: no feedback (NF, blue short dashed), galactic winds (W, green long dashed), standard AGN feedback (AGN1, red dot-dashed), modified AGN feedback (AGN2, cyan solid). For reasons of clarity, we show with errorbars the r.m.s. scatter over the ensemble of simulated clusters only for the AGN1 runs. Observational points refer to the Chandra data analysed by Rasmussen & Ponman (2007) (left panel) and to the Suzaku data analysed by Sato et al. (2008, 2009a, 2009b) (right panel). The two horizontal lines show the relative abundance from SNe-Ia and SNe-II, computed for a simple stellar population (SSP) having solar initial metallicity and based on the same Salpeter IMF and set of yields as used in our simulations.

back (NF runs), including only the effect of galactic winds powered by supernova (SN) feedback (W runs), and including two different prescriptions of AGN feedback (AGN1 and AGN2) based on modelling gas accretion on super-massive black holes (BHs) hosted within resolved galaxy halos (Springel et al. 2005; Di Matteo et al. 2005). The AGN1 scheme exactly reproduces the original model by (Springel et al. 2005) for the choice of the parameters determining the feedback efficiency and the way in which energy is distributed. As for the AGN2 scheme, it assumes the presence of a radiatively efficient "radio mode" phase when BH accretion is in a quiescent stage (e.g., Sijacki et al. 2007), also distributing energy to the gas particles surrounding BHs in a more uniform way.

The main results of our analysis can be summarised as follows.

(a) AGN feedback significantly quenches star formation rate (SFR) associated to the brightest cluster galaxies (BCGs) at $z \lesssim 4$. At $z = 0$ the SFR in the AGN1 and AGN2 models is reduced by about a factor six. For a massive cluster with $M_{200} \simeq 10^{15}\, h^{-1} M_{\odot}$ we find $SFR(z = 0) \simeq 70 M_{\odot}{\rm yr}^{-1}$, thus not far from current observational estimates (e.g. Rafferty et al. 2006). Although the two variants of AGN feedback produce similar results on the star formation rate, the AGN2 model is more efficient is reducing gas accretion onto BHs. For this scheme, the resulting masses of the BHs sitting at the centre of the BCGs at $z = 0$ are reduced by a factor 3–5 with respect to the AGN1 scheme. Furthermore, increasing the radio-mode feedback efficiency from $\epsilon_f = 0.2$ to 0.8 further reduces the mass of the central BH by about a factor 2.5, while leaving the level of low-z star formation rate almost unaffected.

(b) AGN feedback brings the L_X–T relation in closer agreement with observational results at the scale of poor clusters and groups, thus confirming results from previous simulations based on AGN feedback (Puchwein et al. 2008). However, this is obtained at the expense of increasing the ICM entropy in central regions of groups above the level indicated by observational results (e.g., Sun et al. 2009; Sanderson et al. 2009b). This entropy excess generated in central group regions corresponds in turn to a too low value of the gas fraction.

(c) AGN feedback reduces by 30–50 per cent the fraction of baryons converted into stars, f_{star}, within R_{500}. Simulation results agree well with the observed value of f_{star} at the scale of groups. However, for rich clusters the fraction of stars within R_{500} from simulation ($\simeq$ 30–40 per cent) is larger than the observed one ($\simeq$ 10 per cent).

(d) AGN feedback is quite efficient in pressurising gas in the central regions of galaxy groups, thereby generating temperature profiles which are in reasonable agreement with the observed ones. Despite this success at the scale of groups, temperature profiles in the core regions of massive clusters are still too steep, even after including AGN feedback.

(e) The presence of AGN feedback generates a rather uniform and widespread pattern of metal enrichment in the outskirts of clusters. This is the consequence of the improved efficiency, with respect to the runs without BH feedback, to extract at high redshift highly enriched gas from star forming regions, and, therefore, to enhance metal circulation in the inter-galactic medium.

(f) Radial profiles of Fe abundance are predicted to be too steep at $R \gtrsim 0.1 R_{180}$ in runs including stellar feedback. Their shape is in much better agreement with the observed ones when including AGN feedback. The overall emission–weighted level of enrichment within massive clusters is $Z_{Fe} \simeq 0.5$ and 0.6 for runs with and without AGN feedback, respectively. Such values are generally

larger than those, $Z_{Fe} \simeq 0.3$, reported from ASCA observations (Baumgartner et al. 2005).

(g) The distribution of elements mostly produced by SNe-II over a relatively short time-scale is more clumpy than the Iron distribution, which has a larger contribution from SNe-Ia, that release metals over a long time-scale. This is interpreted as due to the effect of enrichment from stars belonging to a diffuse intra-cluster population. Therefore, simulations predict that a sizable fraction of the ICM enrichment is produced by intra-cluster stars, in line with observational evidences (Sivanandam et al. 2009).

(h) The runs with no feedback (NF) and with galactic winds (W) predict similar patterns of $Z_{\rm Si}/Z_{\rm Fe}$ within R_{500}. Silicon abundance is enhanced in the outer regions by the action of galactic winds, thanks to their efficiency in transporting gas enriched by α elements from star forming regions. AGN feedback has the effect of increasing $Z_{\rm Si}/Z_{\rm Fe}$ as a consequence of the suppression of star formation, which would lock back in stars gas surrounding star forming regions, and of the efficient removal of enriched gas from galactic halos.

(i) In no case we find that profiles of $Z_{\rm Si}/Z_{\rm Fe}$ have a rising trend beyond $\simeq 0.2R_{500}$. No strong conclusion can be drawn from a comparison with data, owing to discrepant indications from different observational results on the radial dependence of $Z_{\rm Si}/Z_{\rm Fe}$. Suppression of star formation with AGN feedback causes $Z_{\rm Si}/Z_{\rm Fe}$ to increase at small radii, $\lesssim 0.1R_{500}$, a feature which is not seen in observational data. This suggests that the implementation of AGN feedback in our simulations may not provide enough gas mixing the central regions of clusters and groups.

Our analysis lend further support to the idea that a feedback source associated to gas accretion onto super-massive BHs is required by the observational properties of the ICM (e.g. McNamara & Nulsen 2007). However, our results also show that a number of discrepancies between observations and predictions of simulations still exist, especially within the core regions of massive clusters. This requires that a more efficient way of extracting and/or thermalising energy released by AGN should be introduced in richer systems. A number of observational evidences exists that AGN should represent the engine which regulates the structure of core regions of clusters and groups. However, observations also provide circumstantial evidences that a number of complex physical processes, such as injection of relativistic particles and of turbulence associated to jets, buoyancy of bubbles stabilised by magnetic fields, viscous dissipation of their mechanical energy, thermal conduction, should all cooperate to make AGN feedback a self-regulated process. In view of this complexity, we consider it as quite encouraging that the relatively simple prescriptions for energy thermalisation adopted in our simulations provide a significant improvement in reconciling numerical and observational results on the ICM thermo- and chemo-dynamical properties.

Clearly, increasing numerical resolution thanks to the ever increasing supercomputing power would require including a proper description of the above processes. For instance, the current implementation of AGN feedback neglects the effect of kinetic energy associated to jets. The typical scales of ~ 20 kpc at which kinetic feedback is expected to dominate within clusters (e.g. Pope 2009) are only marginally resolved by hydrodynamics in our simulations, thus making the assumption of a purely thermal feedback a reasonable one. However, the improved numerical resolution expected to be reached in simulations of the next generation needs to be accompanied by a suitable description of injection of jets, for them to provide a physically meaningful description of the interplay between BH accretion and ICM properties.

The results presented in this paper further demonstrate that different astrophysical feedback sources leave distinct signatures on the pattern of chemical enrichment of the ICM. These differences are much more evident in the outskirts of galaxy clusters, which retain memory of the past efficiency that energy feedback had in displacing enriched gas from star-forming regions and in regulating star formation itself. However, characterisation of thermal and chemical properties in cluster external regions requires X–ray telescopes with large collecting area and an excellent control of the background. While Chandra, XMM and Suzaku will be pushed to their limits in these studies in the next few years, there is no doubt that a detailed knowledge of the ICM out the cluster virial boundaries has to await for the advent of the next generation of X–ray telescopes (e.g., Giacconi et al. 2009; Arnaud et al. 2009).

ACKNOWLEDGEMENTS

We are greatly indebted to Volker Springel for providing us with the non–public version of GADGET-2 . We thank Anthony Gonzalez, Alberto Leccardi, Jesper Rasmussen and Ming Sun for having kindly provided tables of observational data points, and Silvia Ameglio for her help in producing the metallicity maps. We acknowledge useful discussions with Hans Böhringer, Francesca Matteucci, Pasquale Mazzotta, Silvano Molendi, Ewald Puchwein, Elena Rasia, Debora Sijacki, Paolo Tozzi, Matteo Viel and Mark Voit. The simulations have been carried out at the "Centro Interuniversitario del Nord-Est per il Calcolo Elettronico" (CINECA, Bologna), with CPU time assigned thanks to an INAF–CINECA grant and to an agreement between CINECA and the University of Trieste, and at the Computing Centre of the University of Trieste. This work has been partially supported by the INFN PD-51 grant, by the INAF-PRIN06 Grant, by a ASI-AAE Theory grant and by the PRIN-MIUR 2007 grant. KD acknowledges the financial support by the "HPC-Europa Transnational Access program" and the hospitality of CINECA.

REFERENCES

Anders E., Grevesse N., 1989, GCA, 53, 197
Arnaud M., Bohringer H., Jones C., McNamara B., Ohashi T., Patnaude D., Arnaud K., Bautz M., et al. 2009, Astro2010: The Astronomy and Astrophysics Decadal Survey, Science White Papers, no. 4
Arnaud M., Evrard A. E., 1999, MNRAS, 305, 631
Böhringer H., Matsushita K., Churazov E., Ikebe Y., Chen Y., 2002, A&A, 382, 804
Baldi A., Ettori S., Mazzotta P., Tozzi P., Borgani S., 2007, ApJ, 666, 835
Baumgartner W. H., Loewenstein M., Horner D. J., Mushotzky R. F., 2005, ApJ, 620, 680
Bhattacharya S., di Matteo T., Kosowsky A., 2008, MNRAS, 389, 34
Bondi H., 1952, MNRAS, 112, 195
Bondi H., Hoyle F., 1944, MNRAS, 104, 273
Booth C. M., Schaye J., 2009, ArXiv e-prints, MNRAS, in press
Borgani S., Diaferio A., Dolag K., Schindler S., 2008, Space Science Reviews, 134, 269

Borgani S., Fabjan D., Tornatore L., Schindler S., Dolag K., Diaferio A., 2008, Space Science Reviews, 134, 379
Borgani S., Governato F., Wadsley J., Menci N., Tozzi P., Quinn T., Stadel J., Lake G., 2002, MNRAS, 336, 409
Borgani S., Kravtsov A., 2009, ArXiv e-prints, ASL, in press
Borgani S., Murante G., Springel V., Diaferio A., Dolag K., Moscardini L., Tormen G., Tornatore L., Tozzi P., 2004, MNRAS, 348, 1078
Borgani S., Viel M., 2009, MNRAS, 392, L26
Brighenti F., Mathews W. G., 2006, ApJ, 643, 120
Buote D. A., 2000, MNRAS, 311, 176
Buote D. A., Lewis A. D., Brighenti F., Mathews W. G., 2003, ApJ, 595, 151
Cattaneo A., Blaizot J., Weinberg D. H., Kereš D., Colombi S., Davé R., Devriendt J., Guiderdoni B., Katz N., 2007, MNRAS, 377, 63
Cavagnolo K. W., Donahue M., Voit G. M., Sun M., 2009, ApJS, 182, 12
Churazov E., Sazonov S., Sunyaev R., Forman W., Jones C., Böhringer H., 2005, MNRAS, 363, L91
Croston J. H., Pratt G. W., Böhringer H., Arnaud M., Pointecouteau E., Ponman T. J., Sanderson A. J. R., Temple R. F., Bower R. G., Donahue M., 2008, A&A, 487, 431
Dalla Vecchia C., Bower R. G., Theuns T., Balogh M. L., Mazzotta P., Frenk C. S., 2004, MNRAS, 355, 995
Davé R., Oppenheimer B. D., Sivanandam S., 2008, MNRAS, 391, 110
De Grandi S., Ettori S., Longhetti M., Molendi S., 2004, A&A, 419, 7
De Grandi S., Molendi S., 2002, ApJ, 567, 163
de Plaa J., Werner N., Bykov A. M., Kaastra J. S., Méndez M., Vink J., Bleeker J. A. M., Bonamente M., Peterson J. R., 2006, A&A, 452, 397
Di Matteo T., Colberg J., Springel V., Hernquist L., Sijacki D., 2008, ApJ, 676, 33
Di Matteo T., Springel V., Hernquist L., 2005, Nature, 433, 604
Dolag K., Borgani S., Murante G., Springel V., 2008, ArXiv e-prints, MNRAS, in press
Fabian A. C., Sanders J. S., Taylor G. B., Allen S. W., 2005, MNRAS, 360, L20
Fabjan D., Tornatore L., Borgani S., Saro A., Dolag K., 2008, MNRAS, 386, 1265
Finoguenov A., David L. P., Ponman T. J., 2000, ApJ, 544, 188
Fukazawa Y., Makishima K., Tamura T., Ezawa H., Xu H., Ikebe Y., Kikuchi K., Ohashi T., 1998, PASJ, 50, 187
Giacconi R., Borgani S., Rosati P., Tozzi P., Gilli R., Murray S., Paolillo M., Pareschi G., et al. 2009, Astro2010: The Astronomy and Astrophysics Decadal Survey, Science White Papers, no. 90
Giodini S., Pierini D., Finoguenov A., Pratt G. W., Boehringer H., et al. 2009, ArXiv e-prints, ApJ, in press
Gonzalez A. H., Zaritsky D., Zabludoff A. I., 2007, ApJ, 666, 147
Grevesse N., Sauval A. J., 1998, Space Science Reviews, 85, 161
Haardt F., Madau P., 1996, ApJ, 461, 20
Heinz S., Brüggen M., Young A., Levesque E., 2006, MNRAS, 373, L65
Horner D. J., 2001, PhD thesis, University of Maryland College Park
Hoyle F., Lyttleton R. A., 1939, in Proceedings of the Cambridge Philosophical Society Vol. 35 of Proceedings of the Cambridge Philosophical Society, The effect of interstellar matter on climatic variation. pp 405–+
Johnson R., Ponman T. J., Finoguenov A., 2009, MNRAS, pp 469–+
Kaiser N., 1986, MNRAS, 222, 323
Kapferer W., Kronberger T., Weratschnig J., Schindler S., Domainko W., van Kampen E., Kimeswenger S., Mair M., Ruffert M., 2007, A&A, 466, 813
Kay S. T., da Silva A. C., Aghanim N., Blanchard A., Liddle A. R., Puget J.-L., Sadat R., Thomas P. A., 2007, MNRAS, 377, 317
Kay S. T., Thomas P. A., Jenkins A., Pearce F. R., 2004, MNRAS, 355, 1091
Lauer T. R., Faber S. M., Richstone D., Gebhardt K., Tremaine S., Postman M., Dressler A., Aller M. C., Filippenko A. V., Green R., Ho L. C., Kormendy J., Magorrian J., Pinkney J., 2007, ApJ, 662, 808
Leccardi A., Molendi S., 2008a, A&A, 487, 461
Leccardi A., Molendi S., 2008b, A&A, 486, 359
Loewenstein M., Mushotzky R. F., 1996, ApJ, 466, 695
Loken C., Norman M. L., Nelson E., Burns J., Bryan G. L., Motl P., 2002, ApJ, 579, 571
Magorrian J., Tremaine S., Richstone D., Bender R., Bower G., Dressler A., Faber S. M., Gebhardt K., Green R., Grillmair C., Kormendy J., Lauer T., 1998, AJ, 115, 2285
Mazzotta P., Brunetti G., Giacintucci S., Venturi T., Bardelli S., 2004, Journal of Korean Astronomical Society, 37, 381
Mazzotta P., Rasia E., Moscardini L., Tormen G., 2004, MNRAS, 354, 10
McNamara B. R., Nulsen P. E. J., 2007, ARAA, 45, 117
McNamara B. R., Rafferty D. A., Bîrzan L., Steiner J., Wise M. W., Nulsen P. E. J., Carilli C. L., Ryan R., Sharma M., 2006, ApJ, 648, 164
Molendi S., Gastaldello F., 2001, A&A, 375, L14
Moll R., Schindler S., Domainko W., Kapferer W., Mair M., van Kampen E., Kronberger T., Kimeswenger S., Ruffert M., 2007, A&A, 463, 513
Murante G., Giovalli M., Gerhard O., Arnaboldi M., Borgani S., Dolag K., 2007, MNRAS, 377, 2
Mushotzky R. F., 2004, in Mulchaey J. S., Dressler A., Oemler A., eds, Clusters of Galaxies: Probes of Cosmological Structure and Galaxy Evolution Clusters of Galaxies: An X-ray Perspective. pp 123–+
Nagai D., Kravtsov A. V., Vikhlinin A., 2007, ApJ, 668, 1
Nagai D., Vikhlinin A., Kravtsov A. V., 2007, ApJ, 655, 98
Omma H., Binney J., Bryan G., Slyz A., 2004, MNRAS, 348, 1105
Oppenheimer B. D., Davé R., 2008, MNRAS, 387, 577
Osmond J. P. F., Ponman T. J., 2004, MNRAS, 350, 1511
Padovani P., Matteucci F., 1993, ApJ, 416, 26
Peterson J. R., Paerels F. B. S., Kaastra J. S., Arnaud M., Reiprich T. H., Fabian A. C., Mushotzky R. F., Jernigan J. G., Sakelliou I., 2001, A&A, 365, L104
Pfrommer C., Enßlin T. A., Springel V., Jubelgas M., Dolag K., 2007, MNRAS, 378, 385
Ponman T. J., Cannon D. B., Navarro J. F., 1999, Nature, 397, 135
Pope E. C. D., 2009, MNRAS, 395, 2317
Pratt G. W., Böhringer H., Croston J. H., Arnaud M., Borgani S., Finoguenov A., Temple R. F., 2007, A&A, 461, 71
Pratt G. W., Croston J. H., Arnaud M., Böhringer H., 2009, A&A, 498, 361
Puchwein E., Sijacki D., Springel V., 2008, ApJ, 687, L53
Rafferty D. A., McNamara B. R., Nulsen P. E. J., Wise M. W., 2006, ApJ, 652, 216

Rasia E., Mazzotta P., Bourdin H., Borgani S., Tornatore L., Ettori S., Dolag K., Moscardini L., 2008, ApJ, 674, 728
Rasmussen J., Ponman T. J., 2007, MNRAS, 380, 1554
Rebusco P., Churazov E., Böhringer H., Forman W., 2005, MNRAS, 359, 1041
Roediger E., Brüggen M., Rebusco P., Böhringer H., Churazov E., 2007, MNRAS, 375, 15
Romeo A. D., Portinari L., Sommer-Larsen J., 2005, MNRAS, 361, 983
Roncarelli M., Ettori S., Dolag K., Moscardini L., Borgani S., Murante G., 2006, MNRAS, 373, 1339
Ruszkowski M., Enßlin T. A., Brüggen M., Begelman M. C., Churazov E., 2008, MNRAS, 383, 1359
Ruszkowski M., Enßlin T. A., Brüggen M., Heinz S., Pfrommer C., 2007, MNRAS, 378, 662
Salpeter E. E., 1955, ApJ, 121, 161
Sanders J. S., Fabian A. C., 2007, MNRAS, 381, 1381
Sanderson A. J. R., O'Sullivan E., Ponman T. J., 2009a, MNRAS, pp 428–+
Sanderson A. J. R., O'Sullivan E., Ponman T. J., 2009b, MNRAS, 395, 764
Sanderson A. J. R., Ponman T. J., O'Sullivan E., 2006, MNRAS, 372, 1496
Saro A., Borgani S., Tornatore L., Dolag K., Murante G., Biviano A., Calura F., Charlot S., 2006, MNRAS, 373, 397
Sato K., Matsushita K., Gastaldello F., 2009, PASJ, 61, 365
Sato K., Matsushita K., Ishisaki Y., Sasaki S., Ohashi T., Yamasaki N. Y., Ishida M., 2008, PASJ, 60, 333
Sato K., Matsushita K., Ishisaki Y., Yamasaki N. Y., Ishida M., Ohashi T., 2009, PASJ, 61, 353
Schindler S., Diaferio A., 2008, Space Science Reviews, 134, 363
Shakura N. I., Syunyaev R. A., 1973, A&A, 24, 337
Shang C., Crotts A., Haiman Z., 2007, ApJ, 671, 136
Sijacki D., Pfrommer C., Springel V., Enßlin T. A., 2008, MNRAS, 387, 1403
Sijacki D., Springel V., 2006, MNRAS, 366, 397
Sijacki D., Springel V., di Matteo T., Hernquist L., 2007, MNRAS, 380, 877
Sivanandam S., Zabludoff A. I., Zaritsky D., Gonzalez A. H., Kelson D. D., 2009, ApJ, 691, 1787
Snowden S. L., Mushotzky R. F., Kuntz K. D., Davis D. S., 2008, A&A, 478, 615
Springel V., 2005, MNRAS, 364, 1105
Springel V., Di Matteo T., Hernquist L., 2005, MNRAS, 361, 776
Springel V., Hernquist L., 2003, MNRAS, 339, 289
Stadel J. G., 2001, Ph.D. Thesis
Sun M., Voit G. M., Donahue M., Jones C., Forman W., Vikhlinin A., 2009, ApJ, 693, 1142
Sutherland R. S., Dopita M. A., 1993, ApJS, 88, 253
Tescari E., Viel M., Tornatore L., Borgani S., 2009, MNRAS, 397, 411
Thielemann F.-K., Argast D., Brachwitz F., Hix W. R., Höflich P., Liebendörfer M., Martinez-Pinedo G., Mezzacappa A., Panov I., Rauscher T., 2003, Nuclear Physics A, 718, 139
Tormen G., Bouchet F. R., White S. D. M., 1997, MNRAS, 286, 865
Tornatore L., Borgani S., Dolag K., Matteucci F., 2007, MNRAS, 382, 1050
Tornatore L., Borgani S., Matteucci F., Recchi S., Tozzi P., 2004, MNRAS, 349, L19
Tornatore L., Borgani S., Springel V., Matteucci F., Menci N., Murante G., 2003, MNRAS, 342, 1025
Valdarnini R., 2003, MNRAS, 339, 1117
van den Hoek L. B., Groenewegen M. A. T., 1997, A&AS, 123, 305
Vikhlinin A., Burenin R. A., Ebeling H., Forman W. R., Hornstrup A., Jones C., Kravtsov A. V., Murray S. S., Nagai D., Quintana H., Voevodkin A., 2009, ApJ, 692, 1033
Vikhlinin A., Kravtsov A., Forman W., Jones C., Markevitch M., Murray S. S., Van Speybroeck L., 2006, ApJ, 640, 691
Vikhlinin A., Markevitch M., Murray S. S., Jones C., Forman W., Van Speybroeck L., 2005, ApJ, 628, 655
Voit G. M., 2005, Reviews of Modern Physics, 77, 207
Werner N., Durret F., Ohashi T., Schindler S., Wiersma R. P. C., 2008, Space Science Reviews, 134, 337
Wiersma R. P. C., Schaye J., Theuns T., Dalla Vecchia C., Tornatore L., 2009, ArXiv e-prints, MNRAS, in press
Woosley S. E., Weaver T. A., 1995, ApJS, 101, 181
Wyithe J. S. B., Loeb A., 2003, ApJ, 595, 614
Yoshida N., Sheth R. K., Diaferio A., 2001, MNRAS, 328, 669
Zhang Y.-Y., Böhringer H., Finoguenov A., Ikebe Y., Matsushita K., Schuecker P., Guzzo L., Collins C. A., 2006, A&A, 456, 55
Zibetti S., White S. D. M., Schneider D. P., Brinkmann J., 2005, MNRAS, 358, 949